Growth Rates and Habits of Ice Crystals between −20° and −70°C

MATTHEW BAILEY AND JOHN HALLETT

Desert Research Institute, Reno, Nevada

ABSTRACT

A laboratory study of ice crystal growth characteristics at temperatures between −20° and −70°C has been performed at ice supersaturations and pressures comparable with those in the atmosphere using a horizontal static diffusion chamber. Maximum dimension, projected area, and volume growth rates, in addition to habit frequency, have been measured for individual habit types as functions of temperature, ice supersaturation, and air pressure. It was found that from −20° to −40°C and at ice supersaturations in excess of 2%, the most frequent habits observed were platelike polycrystals and plates, the complexity of forms increasing with increasing supersaturation. Columns appear with low frequency in this temperature range for all supersaturations. At low ice supersaturation (1%–2%), the habit consists of thick plates, compact polycrystals, and occasional short columns and is the region with the highest frequency of pristine crystals capable of producing halos.

Just colder than −40°C, there is a marked shift to columnar behavior except at low to moderate ice supersaturation (<10%) where the habit is essentially the same as at warmer temperatures with a small increase in the frequency of short columns. At moderate ice supersaturation (10%–25%), long solid columns and polycrystals with columnar and platelike components are observed. Above approximately 25% ice supersaturation, bullet rosettes, long columns, and column-containing polycrystals are observed, the frequency of bullet rosettes and columns increasing with increasing ice supersaturation. At −60°C and colder, needle forms appear along with columnar forms.

These characteristics are portrayed in a habit diagram as a function of temperature and ice supersaturation and are essentially in agreement with the vast majority of atmospheric in situ observations at these temperatures, both of which depart from the previous habit diagrams at temperatures colder than −20°C compiled by Kobayashi, Magono and Lee, and Hallett and Mason.

Habit growth rates and habit frequencies have been measured at 10° temperature increments. Exponential fits of these results yield functions that can be used to estimate growth rates and habit distributions at intermediate temperatures for ice supersaturations as low as 1% up to the maximum values, which might be encountered in the atmosphere due to ventilation effects, approximately up to 50% above water saturation between −25° and −40°C and extrapolated water saturation colder than −40°C. Within each habit and under identical growth conditions, observed extremes in growth rates for individual crystals in comparison with average values show variances of ±50%, reflecting a variance in aspect ratio that suggests a critical role of crystalline defects in growth characteristics. These results indicate an even more complex behavior of ice crystal habit than that observed between 0° and −20°C, a behavior that depends not only on temperature and ice supersaturation, but also on vapor diffusivity, related to air pressure, and the initial nucleation process.

1. Introduction

At temperatures colder than −20°C, glaciated clouds in the middle and upper troposphere play a critical role in the earth's radiation budget (Mason 2002). Detailed knowledge of ice crystal habit, size, and mass distribution are required for accurate cloud parameterization in global climate models and for the interpretation of remote sensing measurements. In situ aircraft observations of ice crystals have provided a useful but limited view of the relation between habit, temperature, and ice supersaturation in the atmosphere. Temperature and relative humidity measurements performed during crystal collection are at times representative of where the crystals are located following sedimentation rather than where they are grown, leading to a skewed view of the correlation between temperature and habit. The picture is further complicated by situations involving the modification or mixing of crystal habits due to vertical motions and turbulence. Additional ambiguities arise from the measurement of ice supersaturation, especially colder than −40°C because of the long time constant of frost point hygrometers in relation to aircraft speed and the scale of horizontal and vertical inhomogeneities in clouds. The purpose of the present experiment is to grow crystals under controlled conditions and thus explore the forms and growth rates which may occur in the atmosphere at low temperatures from −20° to −70°C, overlapping with laboratory studies at higher tempera-

Corresponding author address: Dr. Matthew Bailey, Desert Research Institute, 2215 Raggio Parkway, Reno, NV 89512-1095.
E-mail: bailey@dri.edu

tures. These observations and measurements should enable growth conditions to be inferred from the observed habit and size distributions in the atmosphere.

A number of habit diagrams describing ice crystals can be found in the literature that stem mainly from early laboratory growth experiments at temperatures warmer than $-30°$C performed by Nakaya (1954), Kobayashi (1957), and Hallett and Mason (1958). These studies used both convective cloud chambers and nonconvective diffusion chambers where crystals were grown on rabbit fur or filaments of plastic or glass, sometimes with the addition of silver iodide smoke particles to stimulate nucleation. These initial experiments revealed the well-known habit transitions that occur between $0°$ and $-18°$C (plates to columns to plates) that exhibit a primary dependence on temperature and secondary dependence on ice supersaturation. Subsequent laboratory growth experiments employing a number of different nucleation methods were performed over the following 40 yr or so, reviews of which can be found in Rottner and Vali (1974), Kumai (1982), and Pruppacher and Klett (1997). While nearly all these experiments confirmed the basic habits of ice crystals between $0°$ and $-20°$C, they showed considerable differences at lower temperatures, often in disagreement with both the initial experiments and atmospheric in situ observations.

In a recent study (Bailey and Hallett 2002), crystals were nucleated and grown at temperatures between $-18°$ and $-42°$C at air pressures commensurate with the *U.S. Standard Atmosphere, 1976* (hereafter Standard Atmosphere). Crystals were grown on clean glass filaments and compared with growth on identical filaments coated with particles of kaolinite and silver iodide. The habit observations from that study when compared with previous experiments revealed that many of the earlier results were heavily influenced by the nucleation method, crystal concentration and supersaturation control (or lack of), and air pressure, which affected vapor diffusivity. A summary follows.

1) Tall diffusion chambers can be convectively unstable at high supersaturation, which alters the temperature and calculated vapor gradients. Temperature gradients at the walls of diffusion chambers are critical to control of supersaturation (Tomlinson and Fukuta 1979). Chambers should be "short" with large width-to-height ratios (width/height > 7) in order to avoid these problems (Elliott 1971) as first used by Hallett and Mason (1958).
2) High crystal concentrations in nebulized cloud experiments resulted in ice supersaturation values well below those assumed, cutting off growth shortly following nucleation and resulting in low supersaturation habit forms.
3) Growth at very low air pressures (much lower than those of cirrus clouds) favor the formation of compact pristine crystals.
4) Glass and kaolinite, compositionally similar to each other and to most naturally occurring ice nuclei, produce similar habits that are essentially in agreement with atmospheric in situ observations at Standard Atmosphere pressures. The habit is predominantly platelike and polycrystalline between $-20°$ and $-40°$C.
5) The use of silver or lead iodide for nucleation, either as smoke or for epitaxial growth, biases the habit in favor of columns and both thin and thick plates ("prisms") when other habit forms would normally appear. Silver and lead iodide, which have crystallographic orientations similar to regular hexagonal ice, should be avoided if the goal is to reproduce habits representative of the atmosphere.
6) Use of the term prism, a somewhat ambiguous term rejected by Magono and Lee (1966) when constructing their habit designation scheme, has resulted in confusion when comparing habit results, thick plate prisms being confused with short column prisms and leading to the designation of the habit at temperatures just colder than $-20°$C as "columnar" or consisting of prisms. In Hobbs (1974), a photograph of a very thick plate grown by Kobayashi is referred to as a "column." Schaefer (1949) describes habit transitions from $-8°$ to $-15°$C as proceeding from hexagonal prisms to thick plates to dendrites; however Kobayashi (1961), Kumai (1982), and others, using different methods of nucleation, have found the habit between $-8°$ and $-12°$C to consist of a mix of short columns, equiaxed crystals, thick plates, and nonhexagonal shapes. Since both thin and thick plates and columns with smooth faces can refract light, the lumped description of prisms does not clearly designate the habit as platelike or columnar.

One factor not discussed there is the effect of rabbit hair as a substrate. The cuticle or surface layer of rabbit hair consists of the scleroprotein, keratin, which is highly insoluble in water and takes the form of tiny scalelike structures with sharp edges and flat planar surfaces that may act as miniepitaxial growth surfaces, generally requiring water saturation for nucleation (Kobayashi 1961). It is interesting to note that Rottner and Vali (1974) grew crystals on human hair in a diffusion chamber at temperatures down to $-23°$C with platelike results very similar to those obtained in the present study at this temperature. Microscopically, human hair has a relatively smooth cuticle in comparison with rabbit hair.

A number of attempts have been made to model ice crystal growth between $0°$ and $-20°$C (Kumai 1982; Takahashi et al. 1991; Chen and Lamb 1994; Nelson and Knight 1998; Fukuta and Takahashi 1999; Wood et al. 2001) based on the assumption that the habit is quasi-cyclical or oscillates from plates ($0°$ to $-4°$C), to columns ($-4°$ to $-8°$C), to plates again ($-8°$ to $-20°$C), and finally back to columns just colder than $-20°$C (approximate temperature ranges given). However, a review of atmospheric in situ and laboratory observations

not skewed by silver iodide between $-20°$ and $-40°C$ (Bailey and Hallett 2002) reveals that the crystal habit consists predominantly of platelike polycrystals such as crossed plates, side plane types, scrolls, gohei twins, spearheads, radiating and irregular assemblages of plates, in addition to irregular polyhedral forms (though not presented in this work, the habit transitions between $0°$ and $-20°C$ were routinely reproduced in our diffusion chamber and in a fall tower). Even at low supersaturation ($<2\%$), the habit is still dominated by compact faceted polyhedra, thick plates, and platelike polycrystals. While some of these platelike polycrystalline forms involve atypical growth along the c axis (gohei twins, spearheads, and scrolls), the majority exhibit component growth predominantly along the a-axis direction (crossed plates, side plane types, radiating and irregular assemblages of plates). Hence, the concept of a successive "oscillation" of ice crystal habit back to columnar form just colder than $-20°C$ does not reflect reality.

The general habit transitions between $0°$ and $-20°C$ do not exhibit a periodicity in any usual sense of the word and contain additional transitions as both a function of temperature and supersaturation (e.g., needles from $-4°$ to $-6°C$ near water saturation and plates to sector plates to dendrites with increasing supersaturation at $-14°C$). The plate regime from $-8°$ to $-20°C$ contains a region where equiaxed crystals are most common ($-8°$ to $-10°C$, approximately) in addition to exhibiting the growth of complex forms such as crossed plates, pyramids, trapezoids, trigonal forms, and other habits of nonhexagonal shapes. Habit changes between $0°$ and $-20°C$ have been interpreted as being due to a temperature dependence of the condensation coefficient α through a surface migration length x_s, which has been measured on the basal face and inferred on the prism face from observed habits (Hallett 1961). Below water saturation, α may be zero, so no growth occurs until a critical ice supersaturation is reached. While this might explain the growth changes between simple plate and columnar forms in this temperature interval, it does not address the appearance of nonhexagonal and polycrystalline forms whose shape may depend on the details of nucleation, which is itself a temperature-dependent parameter (Hallett 1964).

Almost all natural and laboratory-grown crystals contain significant concentrations of defects that can be fully as important in determining crystal properties as the periodic nature of the lattice. The majority of the habit forms observed at temperatures colder than $-20°C$ are indicative of nucleation processes that lead to the formation of irregular polycrystals and crystal twins, crystals with two or more components growing from a common grain boundary dislocation (Kobayashi et al. 1976; Furukawa and Kobayashi 1978; Furukawa 1982). Observations of freezing of drops (Hallett 1964; Kobayashi et al. 1976) reveal that most drops freeze as polycrystals below $-20°C$, which is commensurate with

a substantial increase in the observation of twins both in situ and in the laboratory. Laboratory studies of ice growth following heterogenous nucleation by seeding of supercooled drops with clay particles have also been shown to result in a predominance of polycrystalline forms (Yamashita et al. 1984).

Burton et al. (1951) predicted that at low supersaturation, crystals grew through the migration of adsorbed molecules to growth steps on the surface resulting from dislocations. For the case of a screw dislocation with widely spaced spiral steps, growth occurs only from the edge of the steps with no growth at all occurring on the flat interior surfaces beyond a mean molecular migration distance from the edges, indicating that the condensation coefficient is zero on these surfaces (Burton et al. 1951; Hallett 1961). Growth proceeds with steps advancing in width as the spiral evolves. With increasing supersaturation, the steps form a tightening spiral and the role of migration decreases, the growth rate controlled by vapor and heat diffusion alone. Hallett (1961) and Mason et al. (1963) applied these ideas to the growth of the basal plane with measurements showing that the migration distance was related in a complicated way to temperature and could be considered to be key in determining the habit.

Polycrystalline forms often grow simultaneously along principal axes in addition to other directions and have complicated layered structures. Plates typically have imperfect faces that result from successive layer nucleation, each layer advancing at different speeds, often with different thicknesses. Time lapse photography of growth performed in this study reveals that layers of a few micrometers thickness often advance irregularly at different speeds, growing for some distance and then slowing or stalling for some period, only to resume growth again at a different speed. Hence the growth of such crystals would be characterized by a time integration over changing condensation coefficients or migration distances depending on the surface step structure, supersaturation, and presence of defects (possibly influenced by capture of an aerosol particle). The concentration and type of defects that form during nucleation and growth may be even more important in determining the habit of ice crystals, especially below water saturation and in the case of polycrystalline forms. A proper understanding of the correlated nature of all these factors will probably not be achieved until time-resolved lithographic techniques (e.g., X-ray topography) become available that can be applied during crystal growth.

While detailed knowledge of the role of microscopic defects in ice crystal growth is still forthcoming, the laboratory measurement of macroscopic characteristics such as habit, habit distribution, and growth rates provide valuable knowledge and insight concerning the role of ice crystals in the atmosphere. Colder than $-20°C$, habit transitions as functions of both temperature and supersaturation occur, the knowledge of which is critical to modeling the microphysical and radiative properties
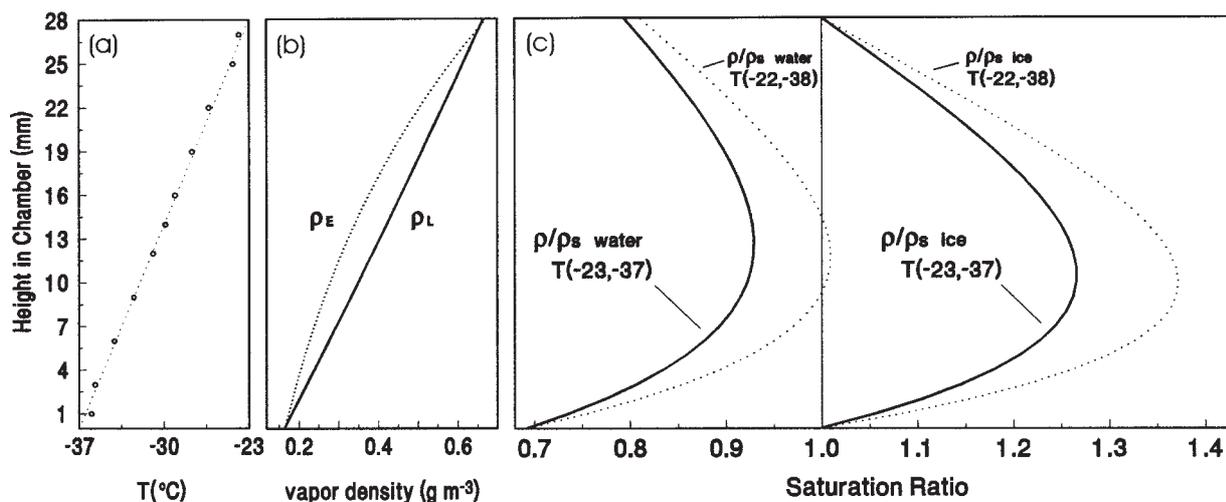
FIG. 1. (a) Temperature, (b) vapor density, and (c) saturation ratio profiles for the diffusion chamber with top and bottom plate temperatures of $-23°$ and $-37°C$, respectively. In (b), both the linear vapor density (ρ_L) predicted by the temperature profile and the equilibrium vapor density over a growing crystal (ρ_E) predicted by the Clausius–Clapeyron equation are shown. The resulting saturation ratios over ice and water surfaces, $\rho/\rho s = S$, are presented in (c) and show that the chamber is supersaturated with respect to ice ($S = \sigma + 1 > 1$, $\sigma =$ supersaturation) and subsaturated with respect to water ($S < 1$) for these temperatures. The dotted line curves are the results for top and bottom plate temperatures of $-22°$ and $-38°C$, respectively, where it can be seen that the central region of the chamber is just supersaturated with respect to water.

of clouds in addition to the interpretation of remote sensing measurements, especially at visible wavelengths. The previous habit diagrams have generally contradicted the vast majority of atmospheric in situ habit observations at temperatures between $-20°$ and $-40°C$, adding further confusion to the interpretation of observations in this critical region of the atmosphere, which, under some conditions, is affected by a habit transition that leads to a mixed habit profile resulting from sedimentation and vertical motions rather than crystal growth conditions. The following study reveals the growth conditions under which agreement is obtained between atmospheric in situ and laboratory observations in addition to those that create apparent contradictions.

2. Experimental description

A modified diffusion chamber has been developed that overcomes many of the nucleation and growth problems with laboratory setups as outlined in Bailey and Hallett (2002). The chamber used in this study consisted of two horizontal, parallel, ice-coated plates with independent temperature control that were separated by an insulating, short, acrylic cylinder, which yielded a large chamber aspect ratio of width:height = 10:1. The temperature differential between the two plates determines the supersaturation and temperature as a function of height in the chamber (Fig. 1). Crystal growth was recorded with time lapse photography using a microscope and video camera.

Crystals were nucleated and grown on filaments approximately 50–70 μm in diameter drawn from soda-

lime glass, a silica glass containing oxides of sodium, calcium, and aluminum that is similar in composition to the most prevalent types of naturally occurring ice nuclei including kaolinites and fine sand particles. When examined under a microscope, the filaments are seen to have many surface cracks and fissures, which result from rapid cooling and solidification while being drawn. There is observational evidence that ice crystals nucleate from tiny supercooled drops that form on the edges of these features (Bailey and Hallett 2002). The glass filaments exhibited a critical supersaturation for nucleation that varied with temperature. Warmer than $-40°C$, an ice supersaturation near water saturation was typically required to initiate nucleation; while colder than $-40°C$, an ice supersaturation of approximately 25% was sufficient. The results shown in Bailey and Hallett (2002) indicate that the critical supersaturation remains approximately constant at 25% colder than $-42°C$; in reality it decreases slightly. Ice layer temperature changes inside the chamber (due to the simultaneous cooling and warming of the bottom and top plates in order to change the supersaturation) slightly lagged the temperature changes in the plates where temperatures were normally measured under equilibrium conditions. Hence, the actual temperature differences between the ice layers at the point of nucleation were slightly overestimated (by 2%–3%) leading to a similar overestimation of the critical supersaturations, an effect that increases with decreasing chamber temperature due to the decreasing cooling rates that are experienced at low temperatures.

Growth and nucleation pressures in the chamber ranged from 550 mb at $-20°C$ to 150 mb at $-70°C$,

approximately Standard Atmosphere pressures for the given temperatures. Below the critical supersaturation for nucleation on clean glass filaments, a filament was placed in the chamber and the chamber was then slowly evacuated to a level near the target pressure. A sudden increase in the evacuation rate was performed when the pressure was approximately 5–10 mb above the target value, leading to a brief adiabatic expansion, which just raised the supersaturation to the critical level, followed by growth under the preset ambient conditions. This process allowed control of the nucleation such that well-separated crystal growth sites could be established that avoided competition for vapor between neighboring crystals. Above the critical supersaturation, a higher density of nucleation sites could result in crowded growth conditions. This could be avoided by retracting the glass filament into a housing on the top plate where nucleation could be prevented until the chamber growth pressures were established. Nucleation occurred once the thread was lowered into place, the most active sites on the thread nucleating first, which gave some crystals a head start on others and allowed them to grow away from the substrate before others had nucleated. These crystals were essentially free from vapor competition, while those that nucleated later were "shadowed" by overhanging crystals, which reduced the supersaturation below the ambient level for the particular vertical position in the chamber. At high supersaturation, nucleation was vigorous and shadowing was difficult to avoid, though some crystals still managed to get ahead of the rest in the initial growth stages and were able to grow relatively free of vapor competition.

3. Experimental results

a. Habit descriptions

With a vertically suspended filament in the chamber, a variety of crystal habits were simultaneously observed with crystals at different heights growing under different conditions of temperature and ice supersaturation. While the supersaturation in the atmosphere rarely exceeds water supersaturation by more than a few percent, ventilation of a crystal due to sedimentation can significantly enhance the mean vapor density gradient around the ice crystal, giving rise to a higher effective supersaturation in comparison with what would be experienced by a stationary crystal growing at ambient conditions. Therefore, growth results for ice supersaturations ranging from 1% to water saturation or considerably above were obtained in order to account for ventilation effects. The habit and growth rate data presented in this section at particular temperatures typically contain crystals that grew within 1°–2°C of the stated temperature. This results in a negligible change in supersaturation since crystals were observed in the midregion of the chamber, a region where the supersaturation varies least with a change in height (Fig. 1).

Many of the habits observed in this study and in situ can be described with the Magono and Lee snow crystal classification scheme, though some polycrystalline forms are not included in their classification and are representative of common types of crystals that occur at low temperature, examples of which are shown in Fig. 2 (a glossary of crystal habits discussed here and later in the paper can be found in the appendix). In the platelike regime from −20° to −40°C, polycrystals of the side plane type (Magono and Lee 1966: S1, S2, and S2S; this paper: sdpl) are often observed, though they may be specific cases of a more general class of polycrystals consisting of "twins," polycrystals which contain a reflection and/or translational plane between components. Twin components grow independently from a grain boundary, the interface between two or more contiguous crystals whose crystallographic orientations differ (twins, in our usage, are not limited to two components). Grain boundaries are a consequence of growth processes in which crystallization begins independently with several different crystallographic orientations rather than just one (Bennett et al. 1965), as occurs when a drop freezes as a polycrystal. In such a nucleating ice embryo, crystallizing components with differing crystallographic orientations, rotated and/or translated with respect to each other, can form stable growth structures if the rotation or translation results in lattice mismatches that are of favorably low energy.

At the molecular scale, the grain boundary consists of an array of dislocations resulting from lattice mismatches (Furukawa and Kobayashi 1978). Microscopically, twin components are observed to originate from a twin boundary structure (referred to hereafter as the TBS), across which there is a change in crystallographic orientation [for "convenience," Furukawa and Kobayashi referred to the TBS as a grain boundary dislocation (GBD); however, like them, we wish to clearly distinguish this microscopic structure from the structure of lattice dislocations at the molecular scale that constitute a grain boundary]. The TBS is usually clearly discernible in photographic images and the details of its structure depends on the type of twin. In simple twins, the component crystals that grow from these structures have specific crystallographic orientations with respect to each other and the TBS, while in more complex twins (side plane types in particular), the orientations can vary.

One of the common types of twins is the "crossed plate" (abbreviated as "cp" in figures), which in its most symmetric form, resembles the feathered end of an arrow. While appearing to be two interpenetrating, elongated, hexagonal plates crossing along maximum diameters at an angle of approximately 70°, they actually consist of four half-hexagons (c axes perpendicular to the half-hexagons or side planes) growing from a TBS. Crossed plates can also appear as two apparently coplanar half-planes on either side of a TBS or as three half-planes, one half-plane being at approximately a 70° angle with respect to the plane formed by the other two.

FIG. 2. Laboratory and in situ examples of the common types of polycrystals discussed in the text that grow between −20° and −40°C. Examples presented have varying size scales. First ISCCP (International Satellite Cloud Climatology Project) Regional Experiment (FIRE) Arctic Cloud Experiment (ACE) (1998) images were obtained from the NASA Langley Research Center Atmospheric Sciences Data Center.

Crossed plates are first observed to grow at a low ice supersaturation of around 2% and appear more frequently as water saturation is approached.

The side plane types (abbreviated as "sdpl" in figures) described by Magono and Lee appear to be asymmetric forms of the crossed plate crystal with pronounced growth of the TBS and multiple twinning components. The TBS appears dark and irregular, sometimes with only a single side plane, but typically with several pairs of side planes emerging at different angles, often partially overlapping or merging as growth proceeds. Radiating assemblages of side planes consist of multiple twinning boundary structures emerging at various angles from a common growth center, each branch with its own degree of side plane development. While many different examples of these types are presented in Magono and Lee, they all appear to be variations of this theme.

The degree of side plane development and the structure of the side planes in polycrystalline twins is apparently dependent on the details of the structure of the TBS, which shows a supersaturation dependence. At low ice supersaturation (slow growth), the TBS grows as a somewhat regular, sharply defined, linear structure whose thickness is not much greater than the side planes. With increasing supersaturation, the TBS becomes thicker and more irregular in structure and is often considerably thicker than the side planes. Side planes, both in crossed plate and side plane crystal types, typically have irregular surfaces that develop (as revealed by time lapse photography) by repeated nucleation of new layers from the TBS with different thicknesses that advance at different speeds across the broad faces of the side planes.

The "gohei" twin is another polycrystalline habit which exhibits a twinning symmetry quite different from that of the crossed plate and side plane types. It typically consists of two skeletal side planes extending from a TBS but, in this case, the platelike components are due to growth along the c axis, which lies in the plane of each side plane (the side planes in this case are clearly not half-hexagons). The c axis of each component makes an acute angle with respect to the TBS, which favors angles of approximately $38.5°$ or a tip angle of $77°$ (Sato and Kikuchi 1985). The two side planes are not coplanar in this case and have an angle of approximately $165°$ between them, giving the crystal the appearance of being slightly folded along the line of the TBS. The crystallographic orientation of the side planes is confirmed by the fact that they sometimes exhibit the growth of a long scroll at their edges, clearly revealing the direction of the c axis, which lies along the axis of the scroll. The side planes are usually fairly symmetric and the growth of interpenetrating repeated structures is common, the TBS clearly running through each pair of side planes. Gohei twins are first observed to grow at modest ice supersaturation (5%–10%) and appear more often as water saturation is approached;

however, they are not a high-frequency habit. Gohei twins and the much more frequent side plane types have similar growth rates and they are combined in the growth data discussed later in this paper.

A twin similar in appearance to the gohei type but with different symmetry, which is observed both in situ and in the laboratory, has a rectangular shape with corner angles of approximately $90°$ (these crystals have been previously referred to in the literature as "tetragonal in shape" or tetragons; however, we decline to use these terms since they could be misconstrued as implying that this form results from the particular crystallographic system designated as tetragonal in symmetry, which was not the intention of earlier authors). Twins of rectangular shape consist of two right-triangle-shaped halves on either side of a pronounced TBS. They are not planar and also often have scrolls growing along one side. As with gohei twins, the two twin components are usually fairly symmetric; however, on occasion, as with side plane types, asymmetric rectangular twins are observed with only one twin component (a right triangle) growing from the TBS. An excellent laboratory example of this asymmetric form (Keller and Hallett 1982) is shown near top left in Fig. 2, where many small right triangles (half of the "rectangular" twin) in addition to the main right triangle component can be seen to grow from only one side of the TBS. Simple rectangular twins appear with a frequency even lower than that of gohei twins. Another form possibly related to rectangular twins are long scrolls (also shown in Fig. 2), which appear as one edge of a crystal that has a pronounced irregular TBS. Such scrolls are different from those designated by Magono and Lee as type C1i (columnar rather than platelike in appearance) and appear with about the same frequency as gohei twins.

Another polycrystal similar in structure to the gohei twin that generally appears at moderately high ice supersaturations is the "spearhead" type (abbreviated as "sph" in figures), which is distinguished from gohei twins by a tip angle of $54°$ and a dominant growth of the TBS itself, resulting in long spear-shaped crystals often with pronounced small side plane growth. As with repeating gohei twins, some spearheads appear to consist of repeating interpenetrating or overlapping twin units, often rectangular or gohei in shape, with shared crystallographic orientations, while others appear to be more irregular in structure. The habit of the side planes generally reflect the growth habit for the temperature at which the spearheads are observed, growing as thin plates, platelike structures, and scrolls for temperatures warmer than $-40°C$, and as columns or sheaths colder than $-40°C$. The side plane structures can be very symmetric or asymmetric in size, position, and distribution with respect to the TBS. Spearheads with substantial side plane development also have growth rates very similar to those of side plane types and have been included with this group. However, some spearheads have little or no side planes, these "bare spearheads" (ab-

breviated as ''spb'' in figures) having extreme linear growth rates and much less obvious structure to the repeating units that form the TBS.

Some twin crystals can be described as rotational or reflection twins, exhibiting a rotational or reflection symmetry with respect to a specific crystallographic axis or plane in the ice lattice (Furukawa 1982). Another type of ''twinning'' that occurs with ice crystals appears to involve a ''slip'' or translation of crystallographic planes that may result from glide planes, stacking faults or defects that lead to the nucleation of several platelike components emanating from a common growth region. The simplest form of this twin (these might be single crystals so twin is used loosely) that grows at low to modest supersaturation (2%–5%) consists of two overlapping plates of similar size, which grow nearly simultaneously from a common contact region such that their c axes and a axes are parallel but the plates are not superimposed, a slip occurring between the two components at a small angle to an a axis. Hence, the plates overlap and their axes and crystal faces are parallel (''overlapping parallel plates,'' abbreviated as ''opp'' in figures), but the faces are not coplanar. Even if the plate components are somewhat asymmetric, a high degree of crystallographic alignment is still observed. The plates often overlap such that a vertex, or side of one plate, lies near the center of an adjacent plate. When viewed on edge, the component plates appear to be slightly interpenetrating in the contact region. Fukuta (1969) obtained a photograph of a pair of thin overlapping parallel plates, which appears to reveal a slip or translational zone (bottom of Fig. 2). Often appearing in small linear groups of two to four plates, they would easily be confused with simple plate aggregates; however, it is statistically unlikely that two or three plates would aggregate with all their axes parallel. Hence, they can be distinguished from random aggregates by their degree of crystallographic alignment. An example of possible overlapping parallel plates obtained with a low-resolution 2DC probe is shown at bottom right in Fig. 2.

At low to modest ice supersaturation, overlapping parallel plates appear as combinations of thick plates of similar size, though there can be an observable progression of sizes between components which indicates that one of the plates nucleated first, followed by the development of the adjacent component. In the case of three or more overlapping parallel plates in a linear or quasi-linear arrangement, the defect that could result from slip, translation, or rotation probably extends through the intervening component plates, which would explain the extended ''telescoping'' structure of these combinations.

At moderate to high supersaturations (approaching water saturation), another form of overlapping parallel plates appears, which consists of plates radiating from a thin, irregular, layered structure that forms a growth hub for the components. This parallel radiating behavior can be distinguished from the random alignment of radiating assemblages of plates or assemblages of simple plates described by Magono and Lee as type P7a and G6. In lithographic studies of other types of crystals that exhibit slip and translation, the growth hub is observed to consist of several thin layers as if sheared or translated. In the case of radiating overlapping parallel plates, each component appears to nucleate from different layers within the hub, which maintains the crystallographic orientation between slipped layers, the component plates being slightly interpenetrating and noncoplanar when viewed on edge.

There are many variations on the platelike polycrystalline themes just described. Radiating or branching polycrystalline forms are often observed with structures consisting of side plane and crossed plate types in addition to clusters of overlapping parallel plates and the occasional gohei twin or spearhead, examples of which are shown in Fig. 2. In addition to these recognizable forms, there are other polycrystals that can truly be described as ''irregular'' [Magono and Lee (1966): G5 or G6; this paper: irreg], which consist of jumbled arrangements of poorly formed but faceted plates or polyhedra of nonhexagonal shape. At low ice supersaturation, they are often compact and nuggetlike while at high ice supersaturation, they appear as spatially extended forms.

b. Habit distributions

The growth rates presented in this work were obtained from crystals that were generally of sizes ranging from 150 to 300 μm; however, many of the images presented show crystals of larger size for habit clarity. With the limited resolution of the long working distance (25 cm) video microscope system used in this study, crystals as small as 10 μm could be detected but not resolved; however, digital enhancement allowed the resolution of faceted crystals as small as 30–50 μm. As a result of this, polycrystals were clearly distinguished from merged groups of single crystals, which might give the false impression of polycrystalline growth. This was also verified with time lapse analysis, which revealed that both polycrystalline and single crystal habits were well established by the time they are of the smallest resolvable size and that single crystals do not transform into polycrystals under constant growth conditions. Additionally, none of the crystals shown could possibly be aggregates.

1) $T = -20°C$

The habits observed at $-20°C$ and a pressure of 550 mb are shown in Fig. 3 along with habit frequencies. At low ice supersaturation of 1%–2%, the habit is characterized by compact, faceted, irregular polycrystals, thick plates (height/width = $0.2 < h/w < 1$), thick overlapping parallel plates, short columns (length/width
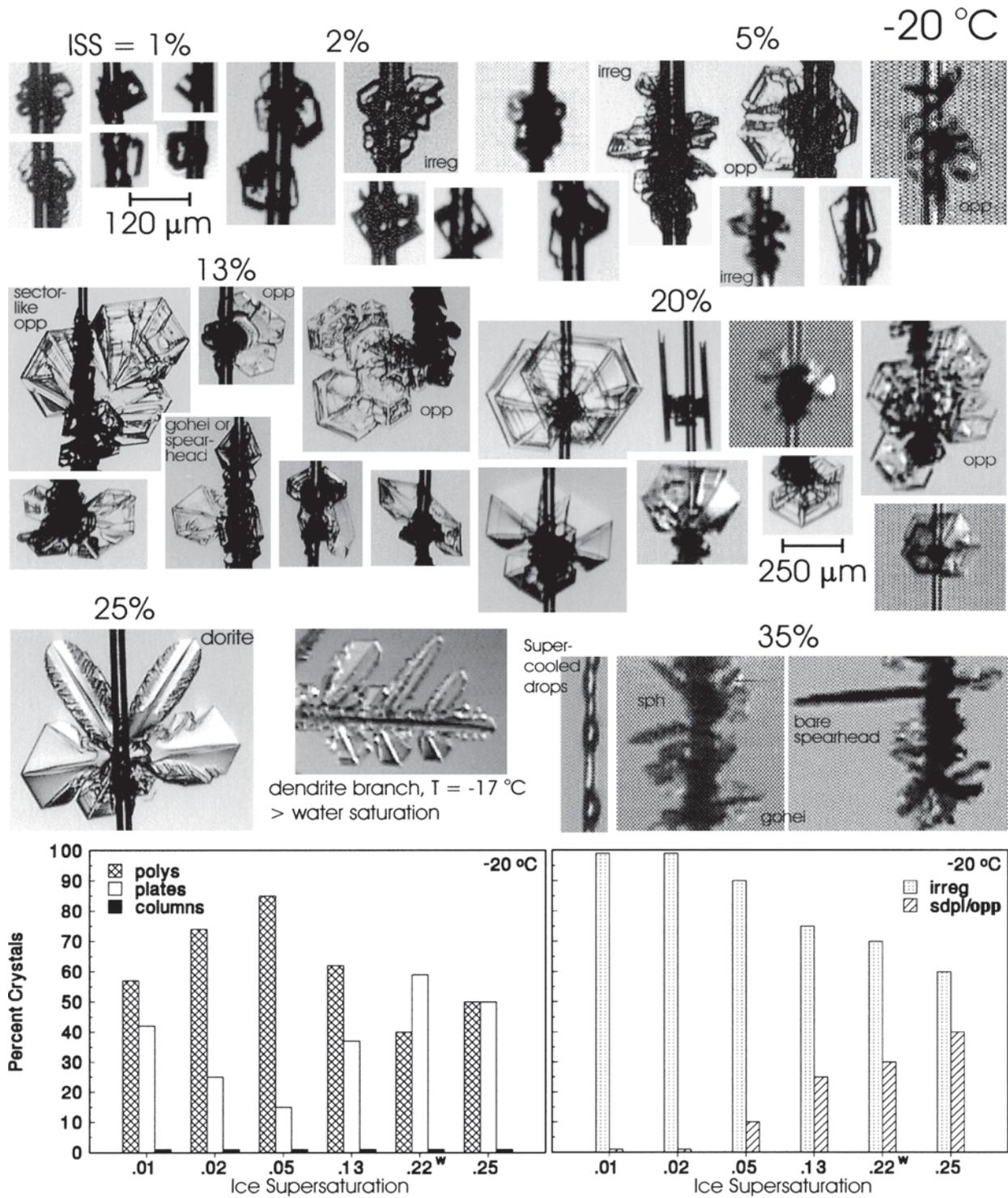
FIG. 3. Habits and habit frequencies of crystals grown at −20°C and a pressure of 550 mb (hPa). Polycrystalline habit frequencies (right side of figure) have been further divided according to habit types discussed in the text. Crystals are shown at different levels of magnification with examples of scale given for habits at 1% and 20% ice supersaturation. In the habit graphs, w denotes the decimal ice supersaturation (σ_w) equivalent to water saturation, approximately the critical supersaturation for nucleation on thin glass filaments.

$= L/w \leq 1.4$) appearing with a frequency of less than 1%, and even rarer equiaxed crystals ($h/w = L/w = 1$). At modest ice supersaturation of 5%–10%, assemblages of thin skeletal plates and large single skeletal plates are the dominant habit. As water saturation (22% with respect to ice) is approached and exceeded, plates become increasingly thin with skeletal and sectorlike structures. The upper part of the assemblage of plates shown at 25% ice supersaturation contains a pair of long thin structures with rounded tips and gently rippled edges, referred to as "dorites" by Hallett and Mason (1958), which appear to be similar to the primary branches of some dendritic forms as in the dendrite branch shown to the right of the dorite, which was grown at $-17°$C (the dorites in the figure emanated from a growth center at a temperature close to $-19°$C; the dorites growing upward toward the region of the chamber at approximately $-17°$C). At 35% ice supersaturation ($\approx 13%$ water supersaturation), assemblages of plates, crossed plates, spearheads, and side planes are commonly observed.

At all ice supersaturations, the majority of hexagonal plates were asymmetric or "scalene" (Hobbs 1974) with sides of different lengths, though not necessarily all different lengths. Scalene plates typically had pairs of sides with equal lengths or trios in the case of crystals with trigonal symmetry. On rare occasions, completely asymmetric plates (six sides with different lengths) were observed. Scrutiny of atmospheric in situ data in the references listed in this paper and elsewhere also reveals these characteristics.

2) $T = -30°$C

The habits observed at $-30°$C and a pressure of 400 mb are shown in Fig. 4. At low ice supersaturation of 1%–2%, the habit is again characterized by compact, faceted polycrystals and thick plates with a modest number of short solid columns. In fact, between $-20°$ and $-70°$C, the low supersaturation habit is essentially independent of temperature with slight increases in the frequency of short columns and irregular or poorly formed plates with decreasing temperature.

Below water saturation (33% with respect to ice), the general habit is still platelike and is dominated by assemblages of plates, overlapping parallel plates and side plane types. Thick crossed plates appear at supersaturations as low as 2%–5% but become thin and much more prevalent as water saturation is approached and exceeded. Plates and platelike polycrystals exhibit more complex skeletal features and greater complexity in general compared with the results at $-20°$C. The polycrystalline assemblages of plates often contain one or more pairs of plates with similar orientation. Figure 4 (upper right) shows what might first be perceived as a bullet rosette developing after nucleation at the critical supersaturation for glass at $-30°$C (Bailey and Hallett 2002) labeled "crit33%." However, the emerging bul-

lets actually developed into a side plane with thick TBS, a short column, and some thick plates. Above this supersaturation value, crossed plates, overlapping parallel plates, and side plane types are the dominant form of polycrystalline growth, spearheads appearing with modest frequency along with gohei twins and short scrolls with length-to-width ratios of about $L/w = 2$–4. At supersaturations in excess of about 75% with respect to ice or about 40% with respect to water, an occasional short sheath or twin scroll is observed. As Figs. 2 and 3 show, many of the platelike polycrystals observed at $-30°$C and, in general, between $-20°$ and $-40°$C, have such complex structures that they are indistinguishable from aggregates observed in situ, bringing into question the degree or frequency of aggregation assumed in many in situ observations.

3) $T = -40°$C

The habits observed at $-40°$C and a pressure of 300 mb are shown in Fig. 5 and are very similar to those at $-30°$C. Irregular assemblages of plates are still the most common habit form, though platelike components are thicker and less extended than at $-30°$C. Solid columns appear with a somewhat larger though still modest frequency and typically have aspect ratio of $1.4 \leq L/h \leq 3$. Crossed plate and side plane types appear with similar frequency as at $-30°$C, though spearheads and scrolls appear with higher frequency at supersaturations above 40% with respect to ice. Short sheaths are occasionally observed at very high ice supersaturations (78%).

The habit from $-20°$ to $-40°$C is platelike; just colder than $-40°$C, there is a dramatic shift to predominantly columnar behavior. Figure 6 shows a number of images of crystal growth on glass filaments where the temperature was approximately between $-38°$ and $-42°$C. Although the details of the habits in this transition region vary with supersaturation, the shift consistently occurs between $-40°$ and $-41°$C for ice supersaturations greater than about 5%. In addition to the habit shift in this narrow temperature range, there is a corresponding drop in the critical supersaturation for nucleation from near water saturation at $-40°$C (47% with respect to ice) to approximately 25% at $-42°$C and colder temperatures (Bailey and Hallett 2002), with bullet rosettes routinely first appearing near the critical value.

4) $T = -42°$ TO $-50°$C

The habits observed at $-50°$C and a pressure of 250 mb are shown in Fig. 7. The 1%–2% supersaturation habit is essentially the same as observed at higher temperatures, solid columns increasing in frequency with increasing supersaturation. Platelike polycrystalline forms are still observed in this temperature region at supersaturations up to 15%; however, this trend de-
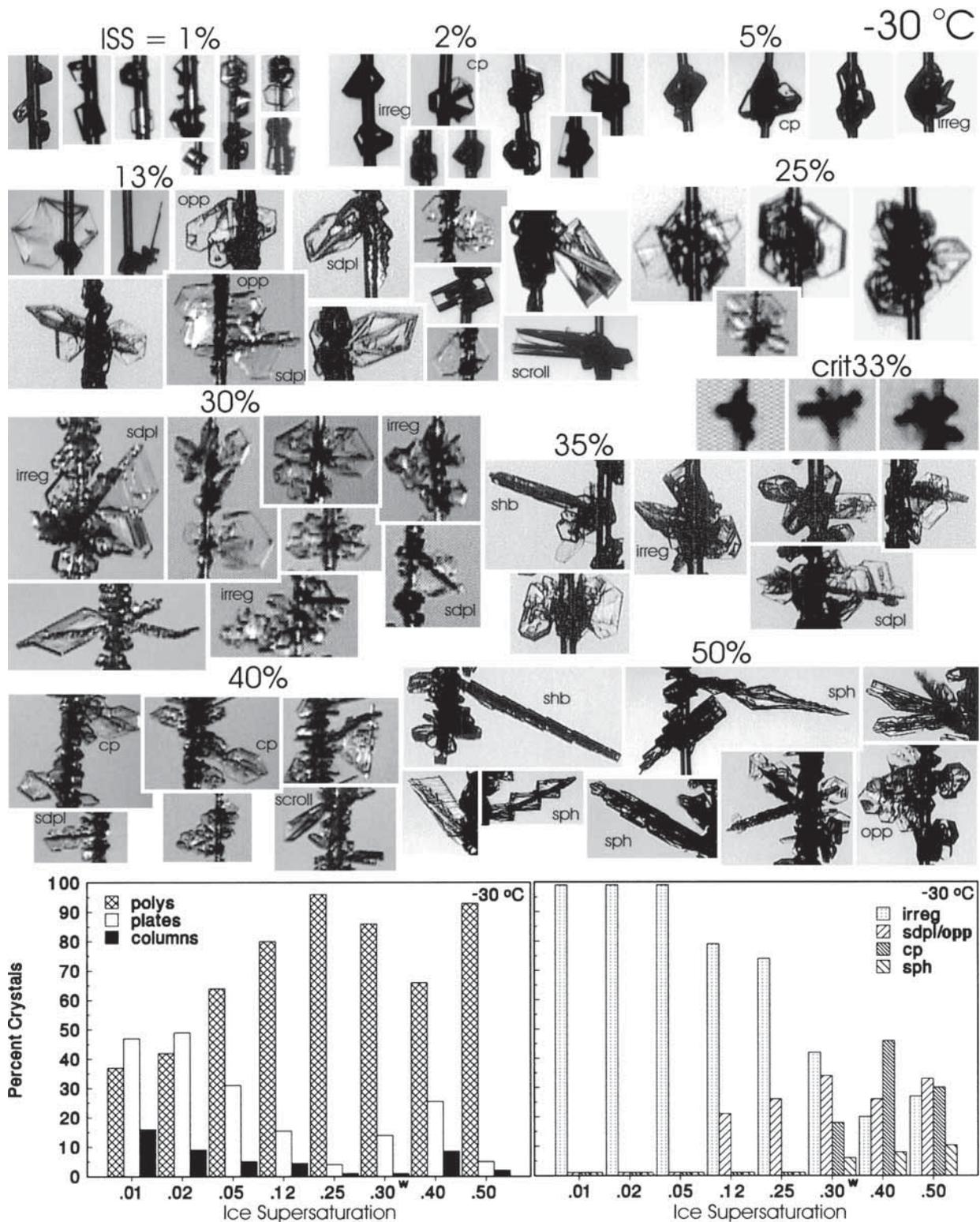
FIG. 4. Habits and habit frequencies of crystals grown at −30°C and a pressure of 400 mb (hPa). Scale is variable as described in Fig. 2. The w in bar graphs denotes the decimal ice supersaturation (σ_w) equivalent to water saturation, approximately the critical supersaturation for nucleation on thin glass filaments.
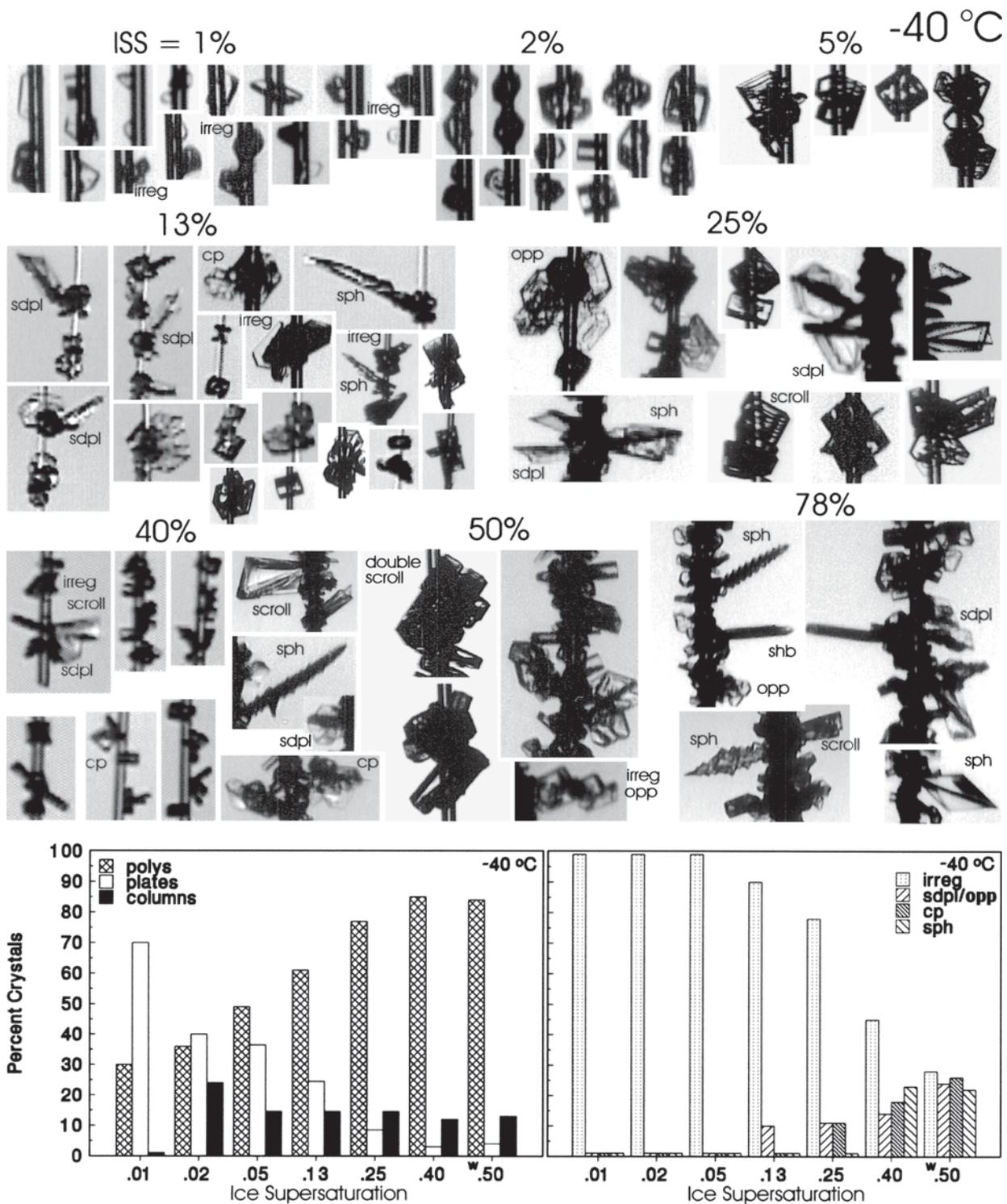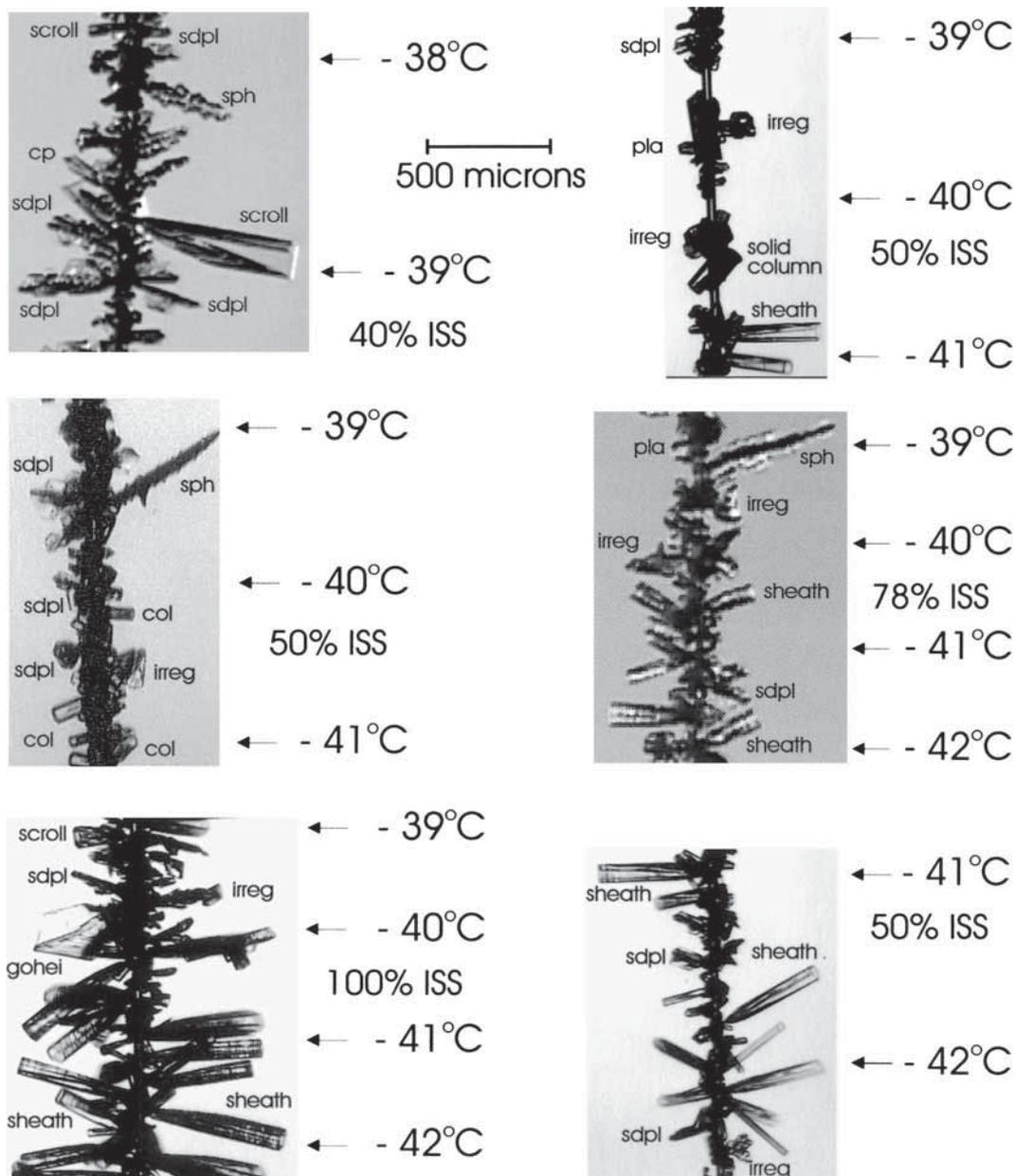
FIG. 5. Habits and habit frequencies of crystals grown at $-40°C$ and a pressure of 300 mb (hPa). Scale is variable as described in Fig. 2. The w in bar graphs denotes the decimal ice supersaturation (σ_w) equivalent to water saturation, approximately the critical supersaturation for nucleation on thin glass filaments.

FIG. 6. Habit observations between −38° and −42°C revealing the transition from platelike to columnar behavior. The transition is essentially independent of ice supersaturation σ. Supersaturation in each image is listed near the temperature to which it corresponds, the supersaturation being somewhat lower above and higher below this position.

creases sharply with decreasing temperature below −50°C. At the critical supersaturation of approximately 25%, bullet rosettes first begin to appear and increase in frequency with increasing supersaturation, becoming the dominant polycrystalline habit. At −42°C and supersaturations of 13%–25%, columns and bullets are solid with aspect ratios of $2 < L/w < 4$, the aspect ratio increasing with both increasing supersaturation and decreasing temperature. Around 40% ice supersaturation, columns and bullets begin to develop hollow ends and become sheaths with increasing supersaturation. Ro-

settes commonly have two to four bullets, three being the average, though rosettes with up to six bullets are observed at times, the average multiplicity of bullets increasing with decreasing temperature and reaching a maximum around −50°C. As previously noted with regard to the scalene quality of most plates, most columns observed in this study were not symmetric in cross section but were scalene, giving the columns a flattened appearance, generally having two wide and four narrower prism faces as depicted in Fig. 8. Tape (1994) described this quality in short columns observed in halo
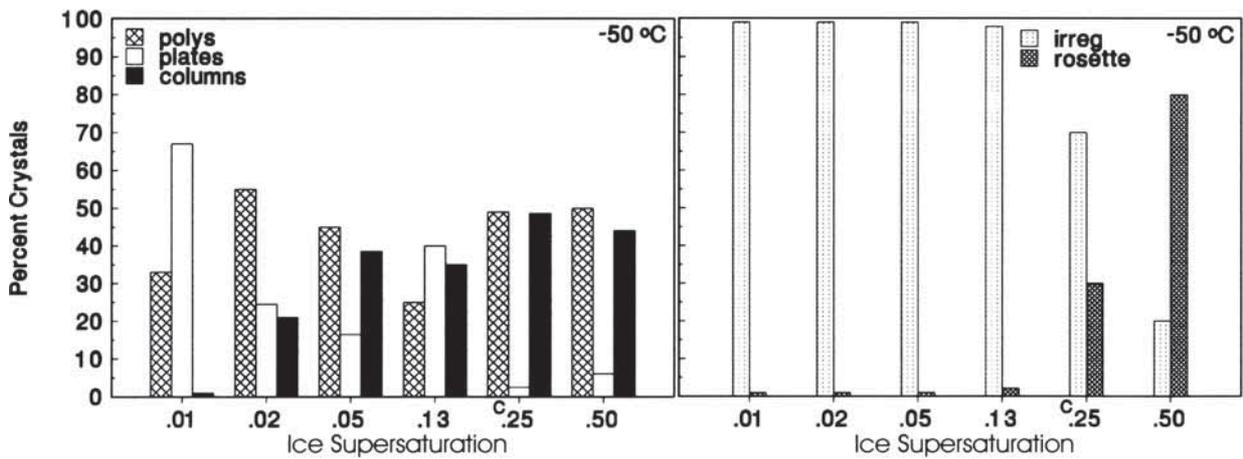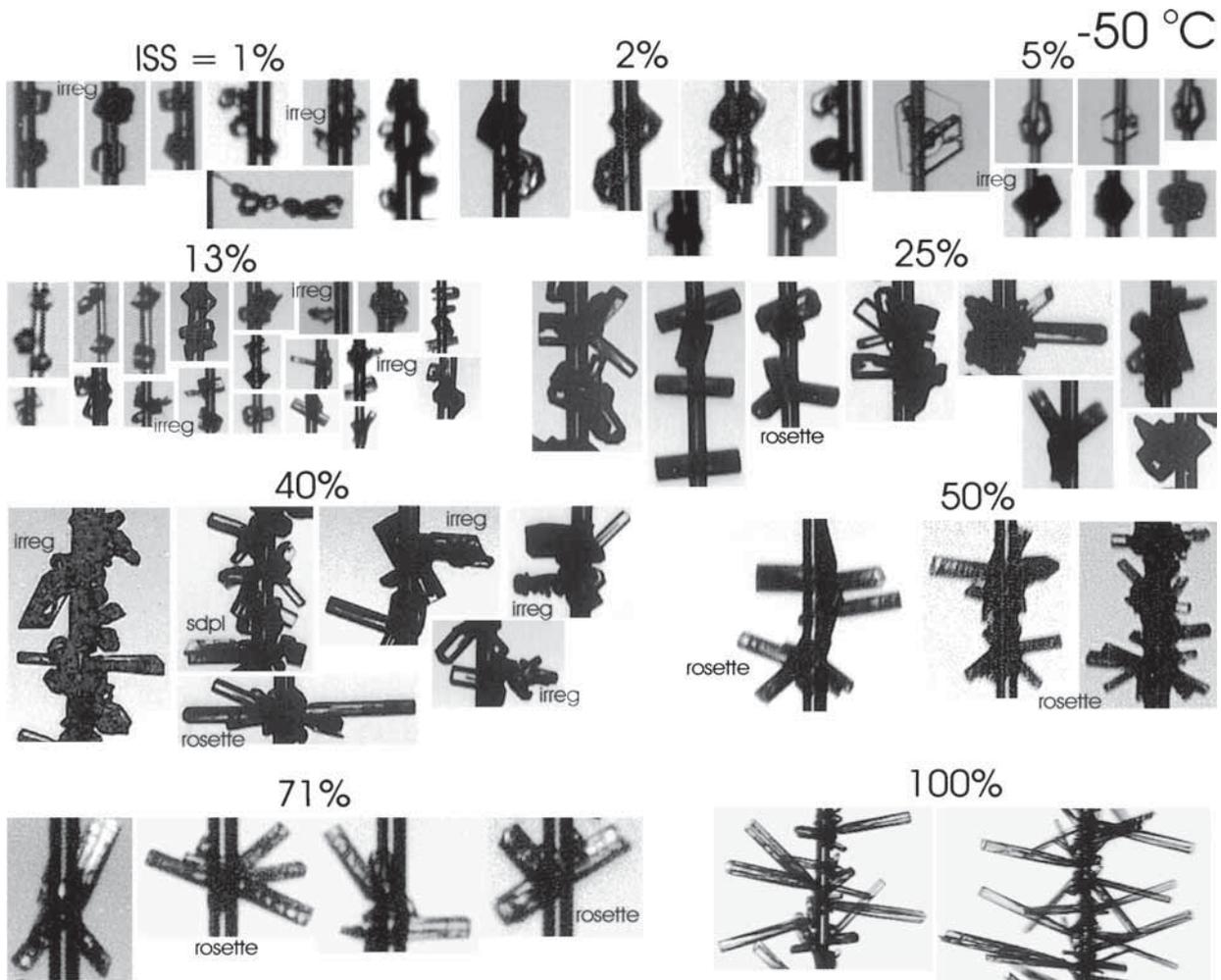
FIG. 7. Habits and habit frequencies of crystals grown at $-50°C$ and a pressure of 250 mb (hPa). Scale is variable as described in Fig. 2. The c in bar graphs denotes the critical supersaturation for nucleation on thin glass filaments ($\sigma_c < \frac{1}{2}$ extrapolated water saturation).

producing crystals in the Antarctic, referring to such crystals as "tabular." However, this flattened behavior is apparent in most of the columns that were collected by Tape in petri dishes of cold hexane where the crystals tend to orient themselves with one of the flattened sides in contact with the bottom of the dish. This effect is not a matter of viewing angle or perspective as can be verified with a symmetrically hexagonal model of a column. No viewing angle can reproduce this flattened appearance. Careful scrutiny of replicator images of natural crystals and other atmospheric in situ data confirms these observations. As with snow flakes, nature appears to favor asymmetric over symmetric forms.

5) $T = -60°C$

The habits observed at $-60°C$ and a pressure of 200 mb are shown in Fig. 9. The low supersaturation habit up to 5% is as previously described; plates are significantly more asymmetric in appearance than at warmer temperatures. At supersaturations of 10%–15%, thick plates and platelike polycrystals appear with about the same frequency as columns that have aspect ratios ranging from $3 < L/w < 6$. Bullet rosettes again begin to appear around a critical supersaturation of 25% with both single columns and bullets being solid, often with aspect ratios $L/w > 6$, the aspect ratio being sensitive to nucleation conditions. If the critical supersaturation is reached quite slowly via a slow change in the temperature differential between the diffusion chamber plates, then the columns that appear are thick and have smaller aspect ratios. If a quick adiabatic expansion is performed near this supersaturation in order to initiate nucleation by raising the effective supersaturation to just above the critical value, the columns tend to be narrower and have larger aspect ratios, up to about 10. This is a general characteristic of column and bullet growth at temperatures colder than $-42°C$ though it is more pronounced at lower temperatures. This implies that the habit of columns or bullet rosettes that nucleate in slow updrafts could be different from those that nucleate under rapidly changing conditions as in strong updrafts or contrails.

At supersaturations around 50%, long columns and bullets appear, sometimes with hollow tips, hollowness increasing with increasing supersaturation. Needlelike forms also begin to appear under these conditions with very large aspect ratios ($L/w \geq 8$), often with prism tips rather than basal faces, and with very flattened appearance, the flattened sides having 3 to 4 times the width of the narrow prism sides (discerned by rotating the substrate and viewing these crystals on end). The thinnest needles with the greatest aspect ratios appear so flattened that the two pairs of narrow sides cannot be resolved with the video microscope, giving an almost rectangular appearance to the needles in cross section. Such crystals have been grown at $-60°$ and then warmed up to $-45°C$, where they obviously regained

their hexagonal cross sections, though this was usually scalene in nature. Needles at $-60°C$ are occasionally observed to grow in overlapping stacks as opposed to the irregular bunches of needles observed near $-5°C$, and they also have a more cleanly faceted appearance than those at $-5°C$.

6) $T = -70°C$

The habits observed at $-70°C$ and a pressure of 150 mb are shown in Fig. 10. The low supersaturation habit up to 5% is similar to that at $-60°C$ (images of crystals at 2% were of too small and of poor quality for display and were analyzed by digital enhancement). The habit at a supersaturation of 13% consisted of compact irregular polycrystals, thick plates, and short columns. At 25% supersaturation, long columns, needles, and needle or columnar rosettes were observed along with unusually shaped crystals (possibly trigonal) consisting of three apparently "pyramid-shaped" bullets, which can be seen in the figure. These crystals bare a strong resemblance to trigonal crystals observed by Heymsfield (1986) in cirriform clouds near $-83°C$ as well as those observed in contrails by Meyers and Hallett (1998) and Hallett et al. (2002) near $-63°C$, where they also appeared in pairs on either side of a central spherical nucleus (frozen drop), rotated so as to give a six-branched appearance. At supersaturations above 50%, needle rosettes, very long needles ($L/w > 10$), and stacks of needles are the most common forms.

c. Growth rates

At high supersaturations, the increased density of growing crystals on a substrate likely reduces the effective supersaturation and observed growth rates. This is due to significant vapor competition between neighboring crystals. However, growth rates in this study were only determined for crystals that were well separated and hence relatively free from vapor competition with neighboring crystals on the substrate. The criteria for this determination came from the mass growth equation for ice particles in an unventilated environment (Hallett et al. 2002), which, to a first approximation, predicts a linear relation between mass growth rate and the ice supersaturation of the environment relative to the surface of a growing crystal:

$$dm/dt = 4\pi C\sigma/(A + B),$$

where C is the electrostatic capacitance of the crystal, A and B are terms representing the effect of heat conductivity and vapor diffusivity on crystal growth (C, A, and B expressed in cgs units), and σ is the ice supersaturation (actually, the equation is linear in the product of C and σ, factors that are discussed later in this section). The supersaturation in this expression is that for a crystal surface at its equilibrium vapor pressure everywhere over its surface and at a slightly warmer tem-
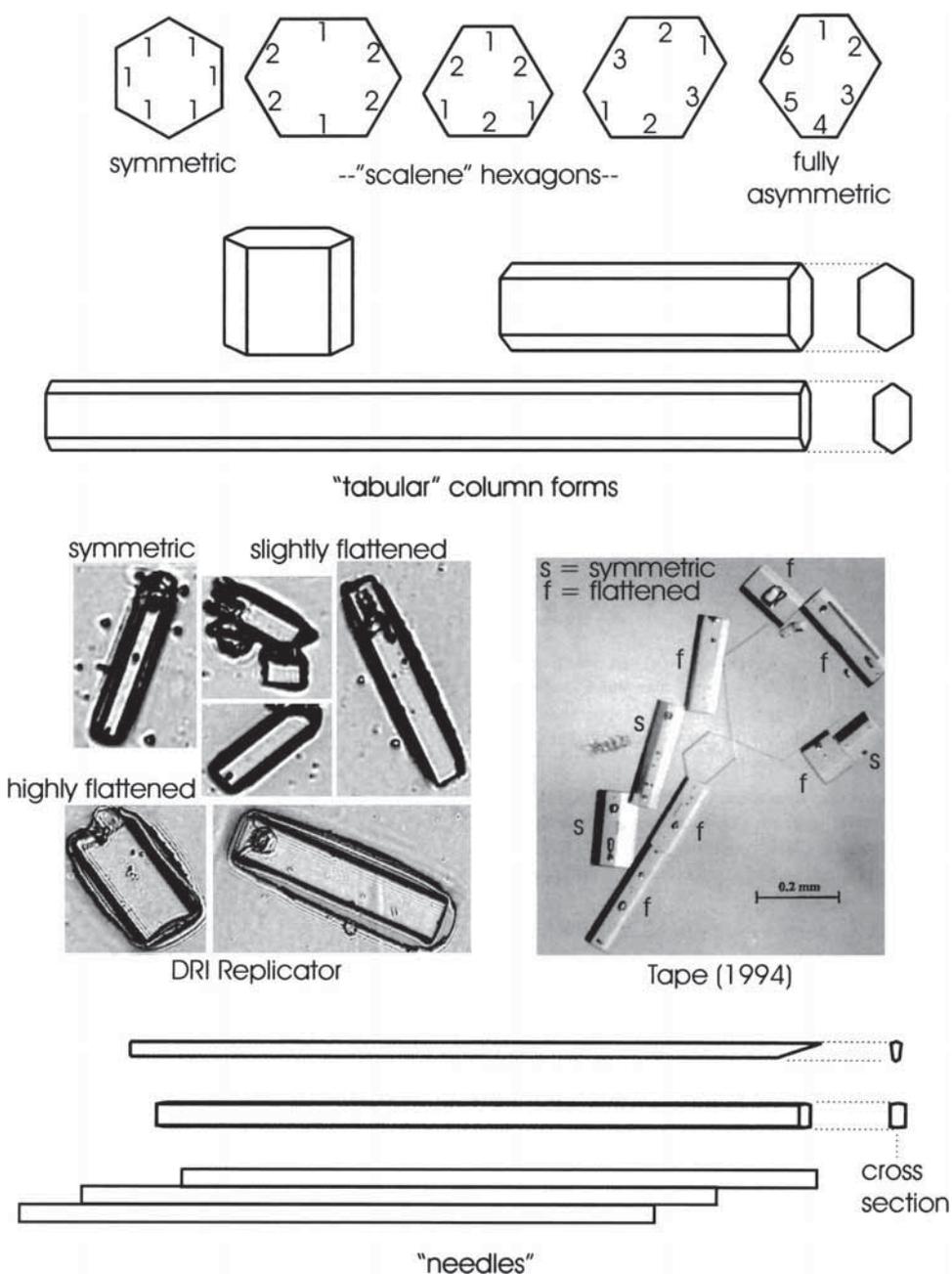
FIG. 8. Asymmetric ice crystal shapes described as scalene plates, flattened or tabular columns and needles or bunches of needles. Numbers listed inside the scalene plates label sides of equal length. Fully asymmetric plates are somewhat rare.

perature than the ambient surroundings due to latent heat release as given by the Clausius–Clapeyron equation. For a particular temperature, the volume growth rates of specific habits were measured at various ice supersaturations and analyzed by linear regression. The slope was essentially constant up to some limiting supersaturation (which was also true of regression slopes for linear and area growth rates), above which it began to decrease (as did its linear correlation coefficient) as

higher supersaturation data were included in the regression, indicating a decrease in the observed growth rate as a function of ice supersaturation, apparently due to vapor competition. The higher supersaturation data were excluded from the regression analysis and results. However, it was observed that, even at these high supersaturations, the few crystals that grew ahead of the others and were not significantly shadowed had growth rates that were still in agreement with the linear results
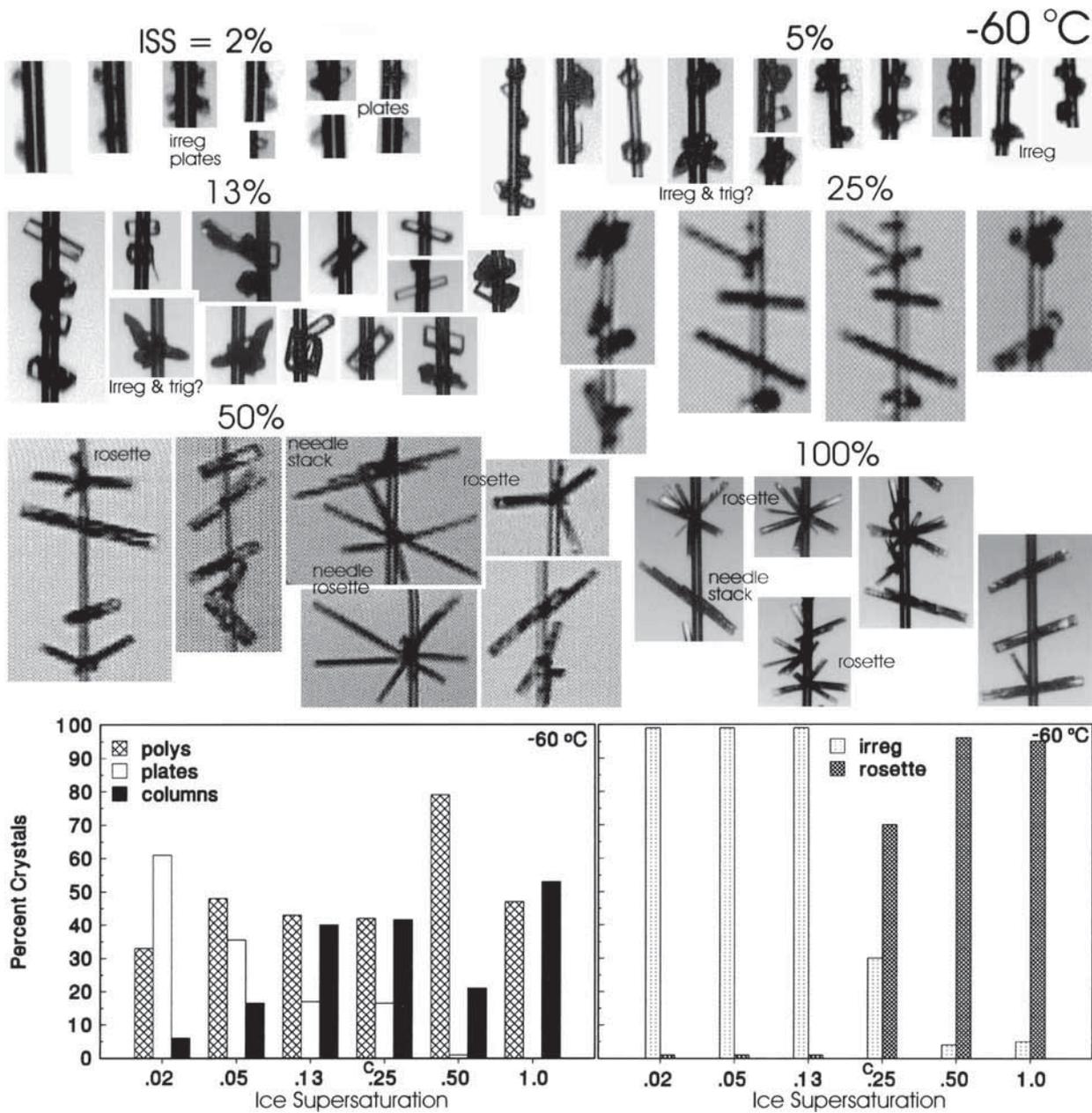
FIG. 9. Habits and habit frequencies of crystals grown at $-60°C$ and a pressure of 200 mb (hPa). Scale is variable as described in Fig. 2. The c in bar graphs denotes the critical supersaturation for nucleation on thin glass filaments ($\sigma_c \ll$ extrapolated water saturation).

at lower supersaturations. Hence, it should be valid to extrapolate growth rates at higher supersaturations from the regression results, especially since habit does not appear to be significantly affected by vapor competition when the values of ice supersaturation are large.

In the mass growth equation presented above, a ventilation factor was not included that reflects an increase in effective supersaturation due to fall through the air as a function of crystal size and shape, related to the square root of the Reynolds number $Re^{1/2}$. For a 300-μm plate falling at 20 cm s^{-1}, this approximately cor-

responds to a 30% increase over the ambient value. As a first approximation, a static diffusion chamber at higher ice supersaturation simulates growth conditions in the atmosphere at lower supersaturation for a crystal falling at constant velocity; however, it cannot reproduce the asymmetric vapor gradients that develop around crystals depending on their shape, size, fall velocity, and orientation during fall.

The capacitance and ventilation factor are both functions of crystal shape and size, which may be modified during the growth history of a crystal. In an unventilated
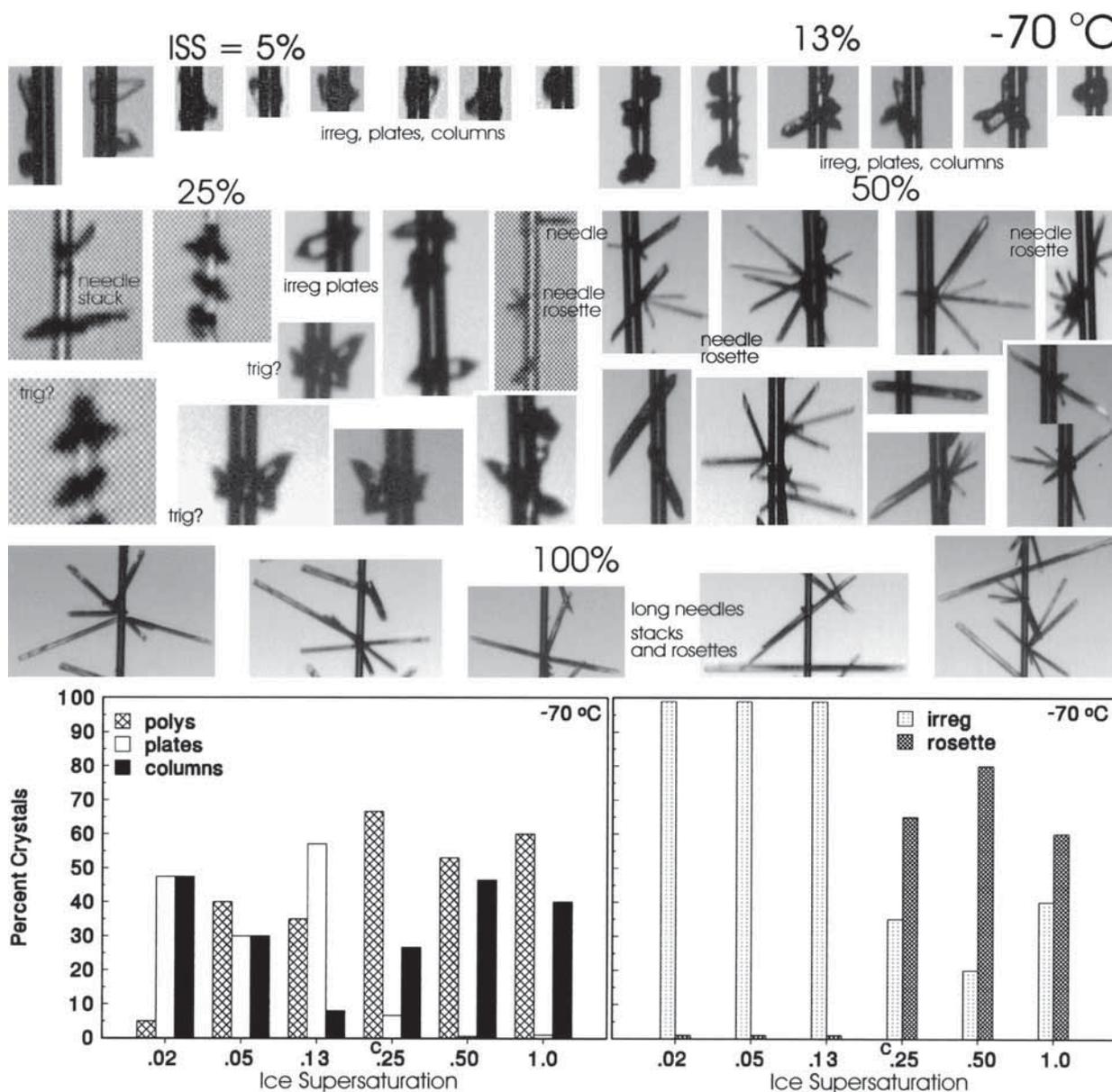
FIG. 10. Habits and habit frequencies of crystals grown at $-70°$C and a pressure of 150 mb (hPa). Scale is variable as described in Fig. 2. The c in bar graphs denotes the critical supersaturation for nucleation on thin glass filaments ($\sigma_c \ll$ extrapolated water saturation).

environment, the mass growth rate depends on the product of capacitance and ice supersaturation. For a constant difference between the vapor pressure or vapor density over the surface of a growing crystal and that of the ambient environment (constant ice supersaturation), the growth equation predicts that the growth rate should increase with increasing crystal size reflected in an increased capacitance. As previously mentioned, growth rates have been calculated for crystals that reached maximum sizes of 150 to 300 μm after some time, and from these measurements, the capacitances of crystals of this size can be calculated. In many other cases, crystals dimensions were measured at various time intervals such that growth rates as a function of time (and changing crystal dimensions) were obtained. Expressions for the capacitances of simple plates and columns, modeled after oblate and prolate spheroids, can be found in the literature (Pruppacher and Klett 1997; Wang 2002). A preliminary analysis of the capacitances of plates and columns of various sizes measured in this study has been performed (a full analysis including more complex habits will appear elsewhere). From these analyses, it is concluded that the electrostatic model severely overestimates crystal capacitances and hence the mass growth rates of crystals. This indicates a breakdown of the electrostatic analogy between a con-

ductor in an electric field (at constant potential) and a growing crystal in a vapor diffusion field where the vapor pressure varies over the surface because of non-growing regions.

In the case of complex shapes with nonuniform vapor density profiles over their surfaces, the capacitance in the growth equation is more like a shape factor that represents the manner in which a crystal responds to the locally variable vapor gradient, which depends on the details of the crystal structure. Some crystal facets may be smooth on a molecular scale and require a critical supersaturation for the two-dimensional nucleation of steps near the crystal edge; for the case of nonthickening molecularly smooth layers advancing over a non-thickening existing crystal, growth occurs entirely by the collection of adsorbed molecules due to surface diffusion, which is demonstrated by the decreasing growth velocity for layers of increasing thickness (Hallett, 1961). The molecules could be collected from the lower or both the upper and lower step, which would give rise to a difference of a factor of 2 in the inferred migration distance (Liu et al. 2002). Facets may also contain emerging dislocations leading to a nonlinear relationship between growth and supersaturation.

For spatially extended polycrystals (e.g., assemblages of plates, side planes, bullet rosettes, etc.), growth near the periphery of a component structure may be faster due to a locally higher supersaturation than that found in the interior where physical obstruction or shadowing of some portions of the crystal occurs. Such conditions are likely to change over time as the crystal evolves in a manner that cannot be reflected by a simple geometric characterization. In the real atmosphere, these conditions are further modified by ventilation with variable fall velocity due to changing mass, shape, and orientation during fall. Ventilation as a function of fall velocity and crystal dimensions can be modeled for simple habits (Wang 2002), but the approach is not suitable for more complex shapes. Effective, habit-specific capacitances are best determined from mass growth rates measured in the laboratory as a function of time and shape (which may still lend themselves to ventilation modeling), yielding time-averaged or time- (and shape-) dependent values that more accurately reflect the response of a crystal to the ambient vapor field.

The growth rates of crystals are plotted in Figs. 11, 12, and 13. Linear growth rates were measured for growth along a maximum dimension dD/dt (diameter or length), which is more relevant than dr/dt (where r is the radius of a spherical ice crystal or the length along a principal axis) since the majority of polycrystals are asymmetric, as are most simple plates (scalene) and columns (tabular). The filament support in the chamber was constructed such that the filament could be rotated about the vertical, allowing crystals to be observed from different angles. Maximum projected area growth rates dA/dt were determined from such analysis, and crystal thicknesses could also be viewed and measured, allow-

ing direct determination of crystal volumes, even in the case of complex crystals with components of differing orientation. The volume growth rates dV/dt can be directly related to the mass growth rate by the ice bulk density ρ (0.92 g cm^{-3}). The growth rates involve fits with anywhere from 10 to 50 independent measurements, depending on the frequency of the habit. So as not to obscure the data, only a few symbols are shown on some of the fits in order to show the spread of growth rates or to clarify which line goes with which habit since some of the growth rates are overlapping or nearly so (e.g., spearheads with side planes ''sph,'' though lower in frequency, have very similar growth rates compared with those of normal side plane types and have been combined).

For results at $-20°C$, sdpl and opp growth rates, as well as those of single plates have been separated into fast (thin platelike) and slow (thick platelike) growth categories; at $-30°C$, plate growth rates have been separated according to symmetric thick, symmetric thin, and asymmetric plates. Both of these reveal that growth rates within a particular habit vary with aspect ratio. Columns are also separated at times according to slow and fast growth forms with small and large aspect ratios, respectively. Irregular crystals are generally of the compact faceted type at low ice supersaturation and are irregular assemblages of plates or plates and columnar forms at temperatures colder than $-40°C$. Spearheads with well-developed side planes are included with side plane types since they have similar growth rates and are distinguished from bare spearheads or ones with little side plane development, which have larger linear growth rates.

An example of the variability of growth rates as a function of aspect ratio is presented in Fig. 14, where the maximum dimension (L), and maximum projected area and volume growth rates for columns at $-50°C$ are plotted against aspect ratio and ice supersaturation. While there is some clustering of growth rates with respect to aspect ratio, there is considerable variability. These results indicate that in addition to temperature and ice supersaturation (the primary factors determining habit), crystal growth is influenced by processes that result in variable aspect ratios, again, a likely reflection of the influence of defects, stress, and/or dislocations in a crystal. Such variability in the aspect ratio of columns in cirrus crystals is commonly observed (Mason 2002).

Bullet rosettes have growth rates that are affected by the multiplicity of bullets and do not scale proportionately with results for single columns. Component bullets observed in the laboratory and in situ are often nonuniform (some being longer than others) and exhibit different aspect ratios and varying degrees of the flattening. Vapor competition among the component bullets, due to shadowing, and orientation during fall may be the reason for these observations.

Regression fits of the growth data yield linear growth rates as a function of, or normalized to, ice supersaturation (Table 1). Within some habits, crystals have been
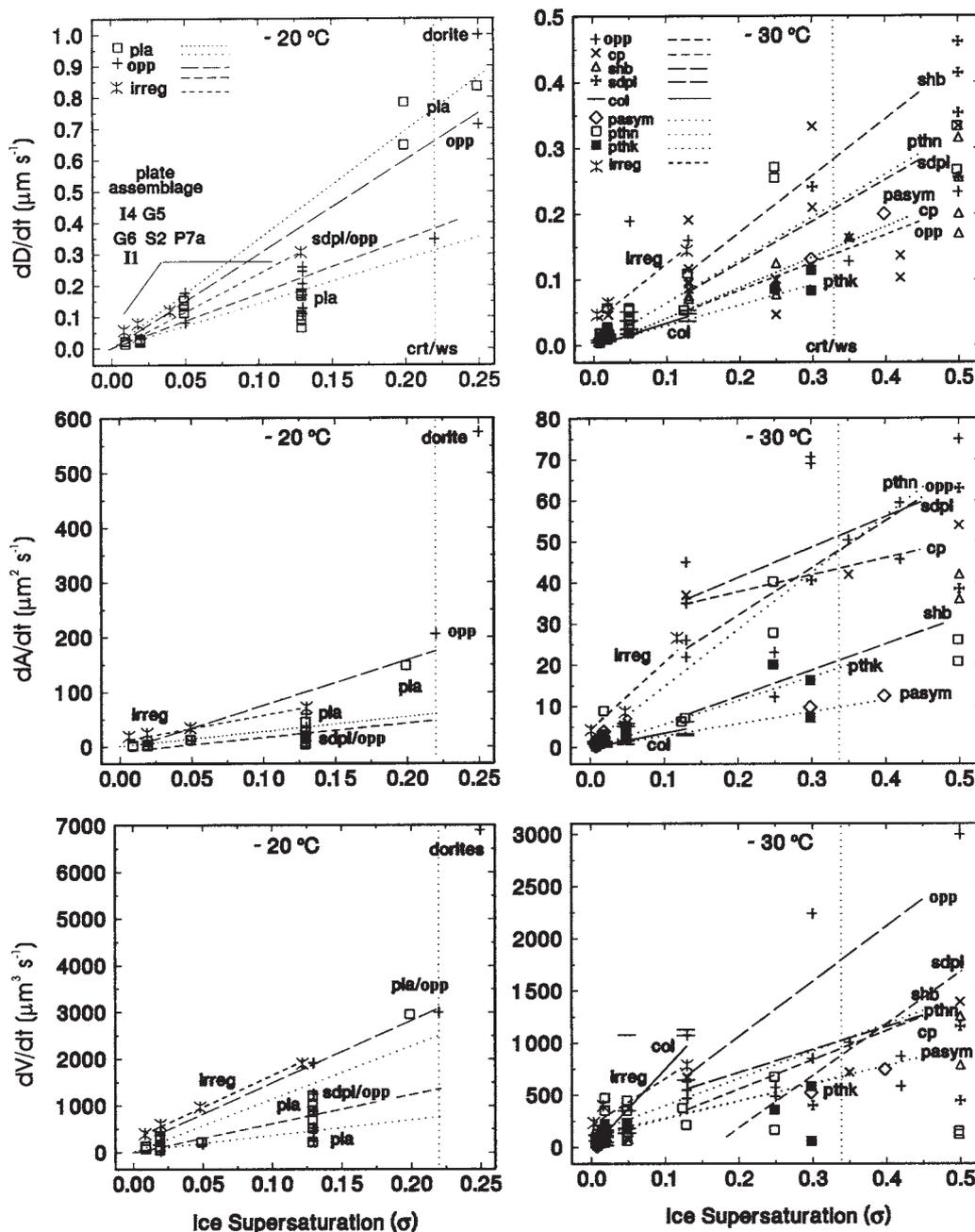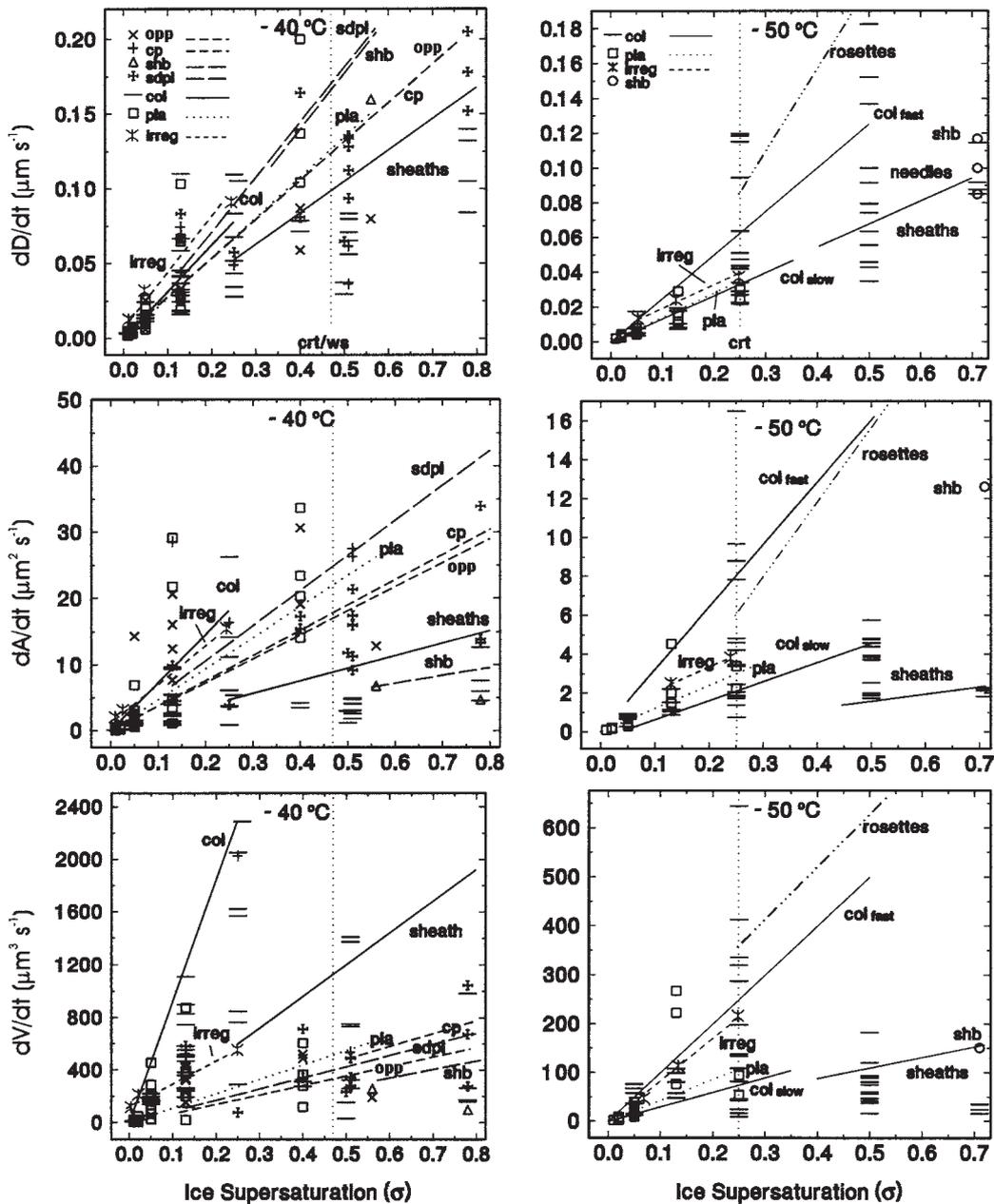
FIG. 11. Growth rates of ice crystal habits at $-20°$ and $-30°C$ for (top) maximum dimension (D), (middle) maximum projected area (A), and (bottom) volume (V).

grouped according to "fast" and "slow," reflecting the variability of growth rate as a function of aspect ratio. To obtain a particular growth rate for a specific habit at a known temperature and ice supersaturation, the product of the slope for this habit and the decimal ice supersaturation yields the growth rate under those conditions; for example, the volume growth rate of a crossed plate growing at $-40°C$ and an ice supersaturation of 30% is equal to 0.30 multiplied by 970 μm^3 $(s\sigma)^{-1}$ or 290 μm^3 s^{-1}. It is interesting to note that,

from $-40°$ to $-70°C$, the columnar regime, columns have the largest average, single crystal, volume growth rates (mass growth rates) when compared with other habit forms, which is not the case in the platelike regime at $-30°C$ except at low ice supersaturation.

d. Average growth rates

A summary of maximum dimension growth rates and habits is presented in Fig. 15, where habit examples

FIG. 12. Growth rates of ice crystal habits at −40° and −50°C.

along with a sample of maximum linear dimension growth rates are presented, again showing the variability discussed in the previous section. A summary of habit distributions is shown in Fig. 16, where it can be seen that polycrystalline forms dominate the habit distribution under most conditions, a result confirmed by extensive atmospheric in situ observations (Heymsfield and Knollenberg 1972; Kajikawa et al. 1980; Korolev et al. 1999, 2000). The top part of the figure shows that single plates were most often observed at low to moderate ice supersaturation (<25%), forming a sort of front wall to the surface in the figure.

While specific growth rates are useful for analyzing or modeling crystal populations of specific habits, in situ crystal populations often consist of a mix of habits, hence growth rates averaged over habit distributions are also of use. Average growth rates normalized to supersaturation were calculated for low to moderate ice supersaturation (<5%; "lo" in Table 1), intermediate (13% up to water saturation for temperatures warmer than −40°C, or the critical supersaturation for nucleation colder than −40°C; "mid" in Table 1), and high supersaturation (in excess of water or the critical supersaturation; "hi" in Table 1) by weighting the nor-
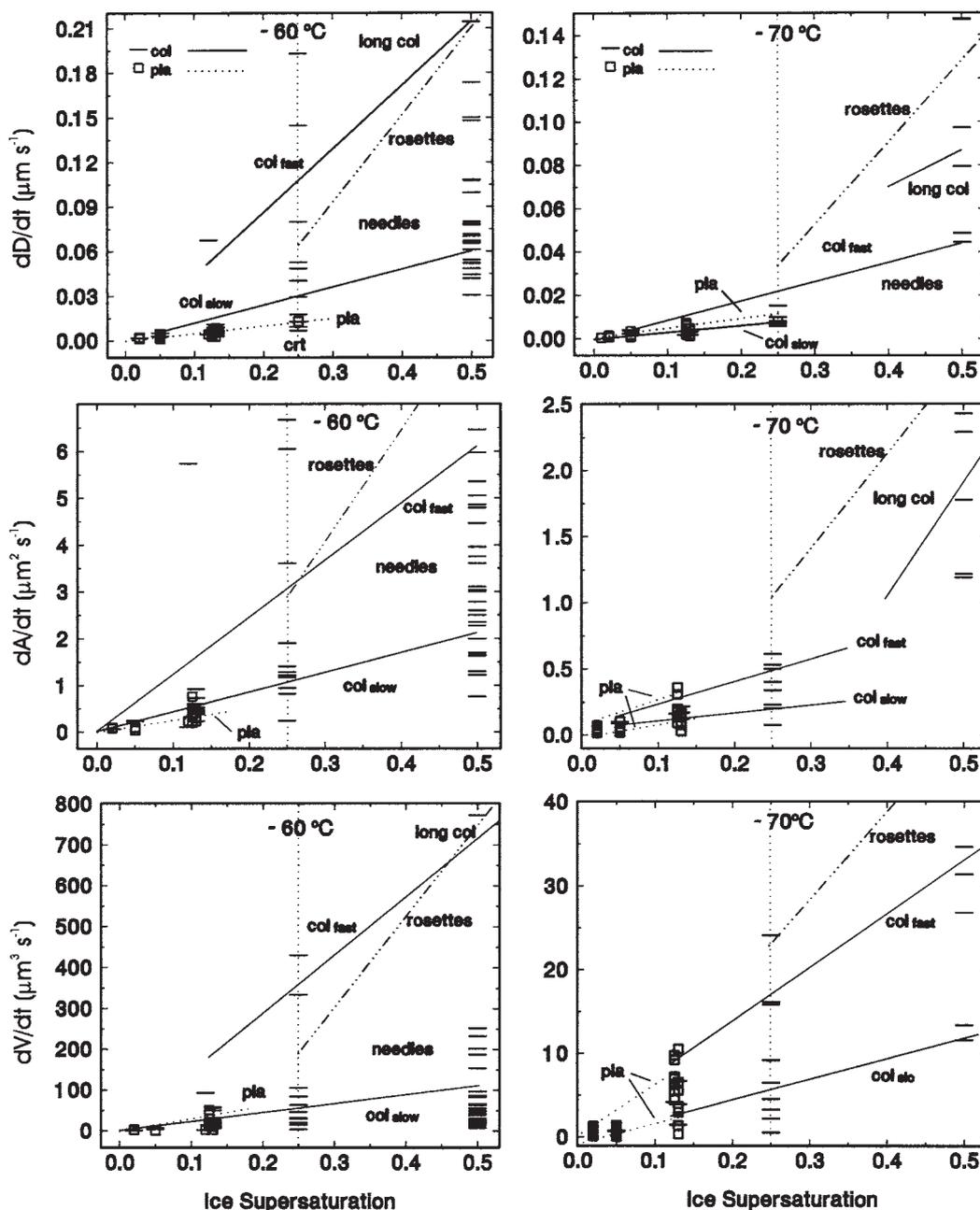
FIG. 13. Growth rates of ice crystal habits at $-60°$ and $-70°$C.

malized growth rates of specific habits by the habit frequency. Intermediate supersaturation results are shown as open circles (dashed curves) in Fig. 17. Growth at supersaturations above water saturation (for $-20°$ to $-40°$C) or the critical supersaturation for nucleation (colder than $-40°$C) often exhibit some of the extreme habits, aspect ratios, and growth rates observed. In order to place upper limits on growth rates, the high supersaturation results have been fitted separately (X symbols and dotted curves) above the dashed curves representing the intermediate supersaturation behavior.

Similarly, very low supersaturation growth results representative of halo crystals (Bailey and Hallett 2002), which consist of pristine plates and columns, have been fitted separately and are shown as open squares (plates) and horizontal bars (columns). The error bars shown with these symbols represent the range of observed growth values (excluding the most extreme) for the particular habit types rather than uncertainties in measured growth rates, which are considerably smaller. The range, once again, reflects the typical variation in aspect ratio and its relation to growth rate. Halo crystals observed
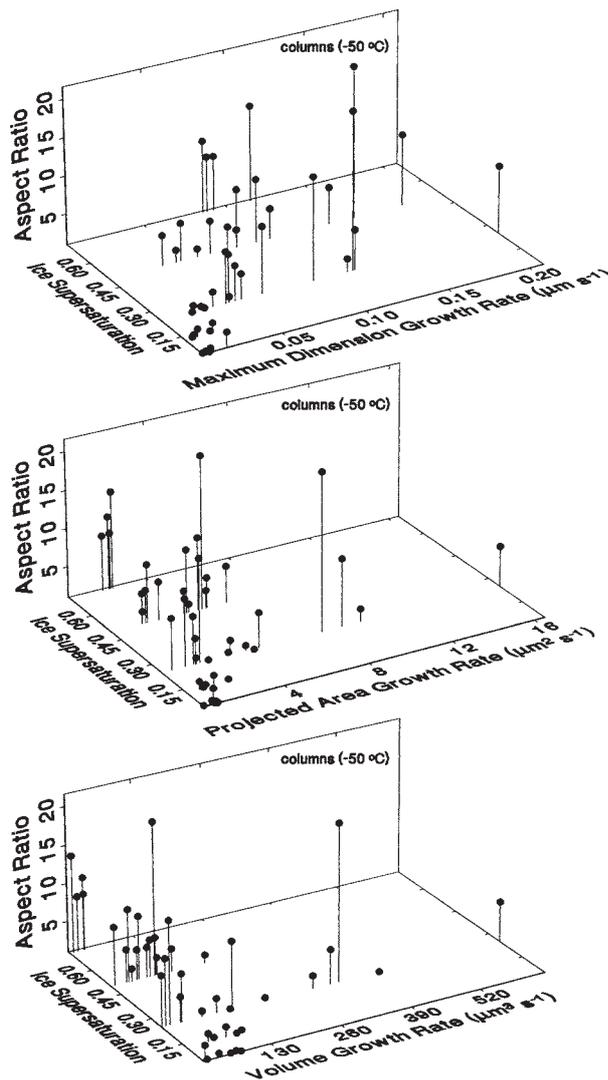
FIG. 14. The variability in growth characteristics of columns at $-50°C$ as a function of aspect ratio.

occurs by two-dimensional nucleation. Additionally, the normalized volume (or mass) growth rates of these crystals is larger than those at intermediate supersaturation, at least for temperatures warmer than $-40°C$, a region characterized by platelike polycrystals with somewhat larger projected area growth rates. This again demonstrates the fact that growth characteristics do not have a simple dependence on temperature and supersaturation but also depend on the details of crystal structure.

4. Comparison with previous laboratory results

There is very little growth data for temperatures colder than $-20°C$ with which to compare the present results, and many previous laboratory studies were done at pressures near 1000 mb, the resulting higher pressure and lower diffusivity affecting the aspect ratio and hence linear dimensional and area growth rates as discussed in the previous section. Additionally, growth rates for crystals grown in fall tower or wind tunnel experiments must be corrected for ventilation effects in order to compare them with stationary crystals grown on substrates. While such an in-depth comparison is beyond the scope of this paper, reasonably good agreement can be observed between the results from this study and those of Ono (1970), Ryan et al. (1976), Yamashita et al. (1984), and Fukuta and Takahashi (1999), as long as these factors are taken into account.

There has been speculation that substrates may perturb habit and/or growth due to thermal conduction effects on facets in contact with the substrate or by inducing defects which stimulate layer nucleation. Nelson and Knight (1998) in a related growth experiment speculated that contact of a crystal facet with a 10-μm-diameter glass capillary stimulated growth since they did not measure a critical supersaturation for growth on such facets. They also noted that crystals usually had a corner or vertex at the location where the capillary penetrated the crystal, a characteristic observed by Kobayashi (1961), in this study, and in others using filament substrates. While corner contact might be evidence for a substrate–crystal interaction, it may simply represent an attempt by an ice embryo or embryonic crystal to minimize stress due to crystallographic mismatch by having minimal initial contact at the vertex of facets. This situation is also likely to occur in the atmosphere when an ice embryo forms either by deposition on an ice nucleus or when a drop freezes heterogeneously due to the presence of a particle where, initially, the embryo or embryonic crystal will be smaller than the nucleus or particle. Natural ice nuclei generally have a weak crystallographic match with ice, and while the crystal must eventually incorporate the particle into its bulk form, it may experience stimulated growth due to stress from such lattice mismatches.

Microscopic confirmation of growth stimulation at the point of substrate contact was not possible in this study but has been observed in epitaxial studies (Bryant et al.

in the polar regions at the ground with pressures near 1000 mb may be expected to have larger aspect ratios due to the effects of diffusivity (Kobayashi 1958; Gonda 1980), which yields thinner extended forms at high pressure (low diffusivity) and more compact forms at lower pressure (high diffusivity). While all the averaged rates show some variability, it is of interest that the normalized maximum dimension growth rates dD/dt of pristine plates and columns at low supersaturation and reduced pressures are approximately the same as those at intermediate supersaturations. This is inconsistent with the prediction of a quadratic dependence on supersaturation for linear growth at low supersaturation predicted by Burton et al. (1951), which would yield much lower growth rates; however, that prediction is expected to be valid for a growing crystal only in contact with its vapor and not in a mixture of air and vapor or when growth

TABLE 1. Maximum linear dimension, projected area, and volume growth rates normalized to ice supersaturation (σ). "Pla" stands for plates, "col" for columns, and "asmb" for assemblage of plates. All other acronyms are defined in text.

-20 °C	$(1/\sigma)dD/dt$ $\mu m(s\sigma)^{-1}$	$(1/\sigma)dA/dt$ $\mu m^2(s\sigma)^{-1}$	$(1/\sigma)dV/dt$ $\mu m^3(s\sigma)^{-1}$
sdpl/opp $_{fast}$	2.7 ± 0.5	1700 ± 520	22000 ± 6000
sdpl/opp $_{slow}$	1.4 ± 0.3	210 ± 35	4200 ± 1300
pla $_{fast}$	3.1 ± 0.4	500 ± 130	19000 ± 4000
pla $_{slow}$	2.0 ± 0.6	400 ± 80	4100 ± 800
irreg/asmb	2.6 ± 0.8	430 ± 80	13000 ± 4000
ave $_{lo}$	2.6 ± 0.3	140 ± 10	11000 ± 2000
ave $_{mid}$	2.2 ± 0.8	280 ± 150	7400 ± 2000
ave $_{hi}$	3.3 ± 0.8	800 ± 200	13000 ± 3000

-30 °C	$(1/\sigma)dD/dt$ $\mu m(s\sigma)^{-1}$	$(1/\sigma)dA/dt$ $\mu m^2(s\sigma)^{-1}$	$(1/\sigma)dV/dt$ $\mu m^3(s\sigma)^{-1}$
opp	0.42 ± 0.12	115 ± 25	5000 ± 1300
cp	0.27 ± 0.09	41 ± 26	2800 ± 1400
shb	0.86 ± 0.10	67 ± 13	2200 ± 500
sdpl	0.63 ± 0.10	75 ± 24	5300 ± 1200
col	0.32 ± 0.06	28 ± 7	2300 ± 700
pasym	0.46 ± 0.02	29 ± 3	700 ± 100
pthn	0.65 ± 0.06	140 ± 10	2600 ± 500
pthk	0.31 ± 0.02	54 ± 8	1600 ± 240
irreg/asmb	0.78 ± 0.15	190 ± 40	4600 ± 800
ave $_{lo}$ pla col	1.27 ± 0.15 / 0.76 ± 0.28	130 ± 10 / 100 ± 65	7500 ± 900 / 9000 ± 2800
ave $_{mid}$	0.62 ± 0.40	140 ± 80	2400 ± 1200
ave $_{hi}$	0.94 ± 0.25	180 ± 40	6000 ± 2000

-40 °C	$(1/\sigma)dD/dt$ $\mu m(s\sigma)^{-1}$	$(1/\sigma)dA/dt$ $\mu m^2(s\sigma)^{-1}$	$(1/\sigma)dV/dt$ $\mu m^3(s\sigma)^{-1}$
opp	0.26 ± 0.03	36 ± 8	720 ± 210
cp	0.28 ± 0.03	38 ± 8	970 ± 170
shb	0.36 ± 0.02	12 ± 3	630 ± 100
sdpl	0.38 ± 0.05	53 ± 8	850 ± 190
col	0.26 ± 0.06	73 ± 11	2200 ± 1000
pla	0.25 ± 0.06	47 ± 7	1100 ± 310
sheaths	0.21 ± 0.03	19 ± 3	2400 ± 400
ave $_{lo}$ pla col	0.35 ± 0.06 / 0.40 ± 0.20	33 ± 11 / 17 ± 8	2100 ± 1400 / 2400 ± 1200
ave $_{mid}$	0.32 ± 0.08	43 ± 10	910 ± 270
ave $_{hi}$	0.38 ± 0.20	55 ± 12	3900 ± 600

-50 °C	$(1/\sigma)dD/dt$ $\mu m(s\sigma)^{-1}$	$(1/\sigma)dA/dt$ $\mu m^2(s\sigma)^{-1}$	$(1/\sigma)dV/dt$ $\mu m^3(s\sigma)^{-1}$
pla	0.14 ± 0.02	12 ± 1	430 ± 40
col $_{slow}$	0.14 ± 0.01	9.6 ± 1.4	300 ± 40
col $_{fast}$	0.25 ± 0.04	32 ± 8	1000 ± 100
sheaths	0.13 ± 0.02	3.7 ± 0.4	220 ± 20
rosettes	0.34 ± 0.10	20 ± 5	2800 ± 600
ave $_{lo}$ pla col	0.47 ± 0.26 / 0.13 ± 0.08	15 ± 5 / 13 ± 10	650 ± 340 / 850 ± 200
ave $_{mid}$	0.26 ± 0.10	9 ± 2	500 ± 70
ave $_{hi}$	0.36 ± 0.10	30 ± 10	2100 ± 400

-60 °C	$(1/\sigma)dD/dt$ $\mu m(s\sigma)^{-1}$	$(1/\sigma)dA/dt$ $\mu m^2(s\sigma)^{-1}$	$(1/\sigma)dV/dt$ $\mu m^3(s\sigma)^{-1}$
pla	0.050 ± 0.003	3 ± 1	340 ± 130
col $_{slow}$	0.12 ± 0.02	2.4 ± 0.2	220 ± 20
col $_{fast}$	0.43 ± 0.20	8 ± 0.6	1400 ± 100
needles	0.22 ± 0.08	4.0 ± 0.3	280 ± 60
rosettes	0.60 ± 0.10	12 ± 3	2600 ± 400
ave $_{lo}$ pla col	0.08 ± 0.05 / 0.09 ± 0.03	2 ± 1 / 9 ± 5	120 ± 85 / 200 ± 50
ave $_{mid}$	0.24 ± 0.18	5 ± 1	220 ± 35
ave $_{hi}$	0.42 ± 0.10	14 ± 2	1100 ± 400

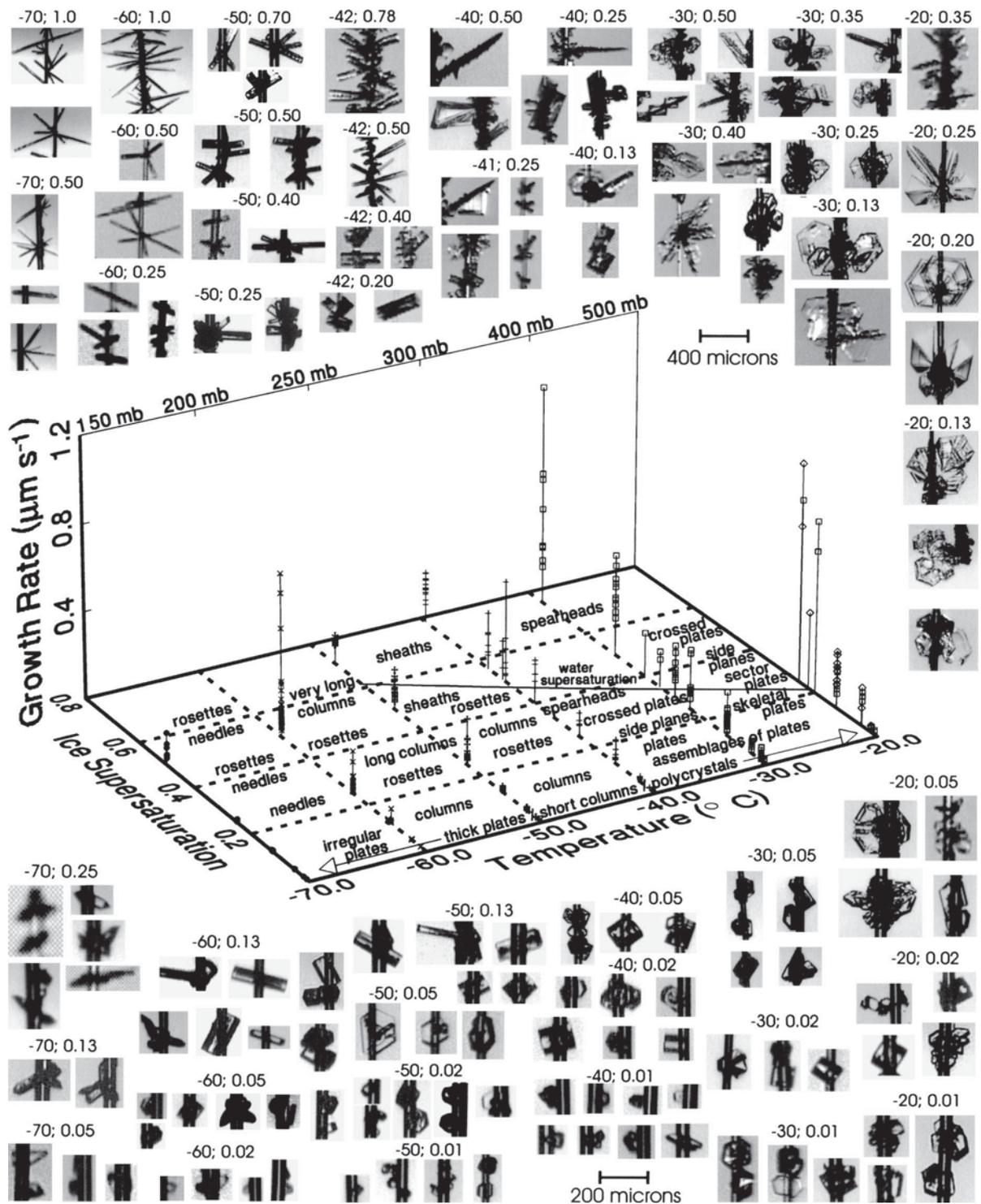| -70 °C	$(1/\sigma)dD/dt$ $\mu m(s\sigma)^{-1}$	$(1/\sigma)dA/dt$ $\mu m^2(s\sigma)^{-1}$	$(1/\sigma)dV/dt$ $\mu m^3(s\sigma)^{-1}$
needles	0.17 ± 0.06	1.8 ± 0.6	69 ± 18
pla	0.045 ± 0.004	1.0 ± 0.3	22 ± 5
col $_{slow}$	0.031 ± 0.002	0.6 ± 0.1	27 ± 5
col $_{fast}$	0.25 ± 0.04	9 ± 2	75 ± 15
rosettes	0.40 ± 0.10	7.5 ± 1.8	85 ± 20
ave $_{lo}$ pla col	0.04 ± 0.02 / 0.05 ± 0.02	2 ± 1 / 6 ± 3	39 ± 20 / 29 ± 10
ave $_{mid}$	0.05 ± 0.02	3 ± 0.3	25 ± 5
ave $_{hi}$	0.29 ± 0.08	6 ± 2	140 ± 35

FIG. 15. Summary of habits and linear growth characteristics as a function of temperature, ice supersaturation, and air pressure. Temperature in °C and decimal ice supersaturation (σ) appear above groups of ice crystals growing under these conditions. Indicated size scales are approximate.
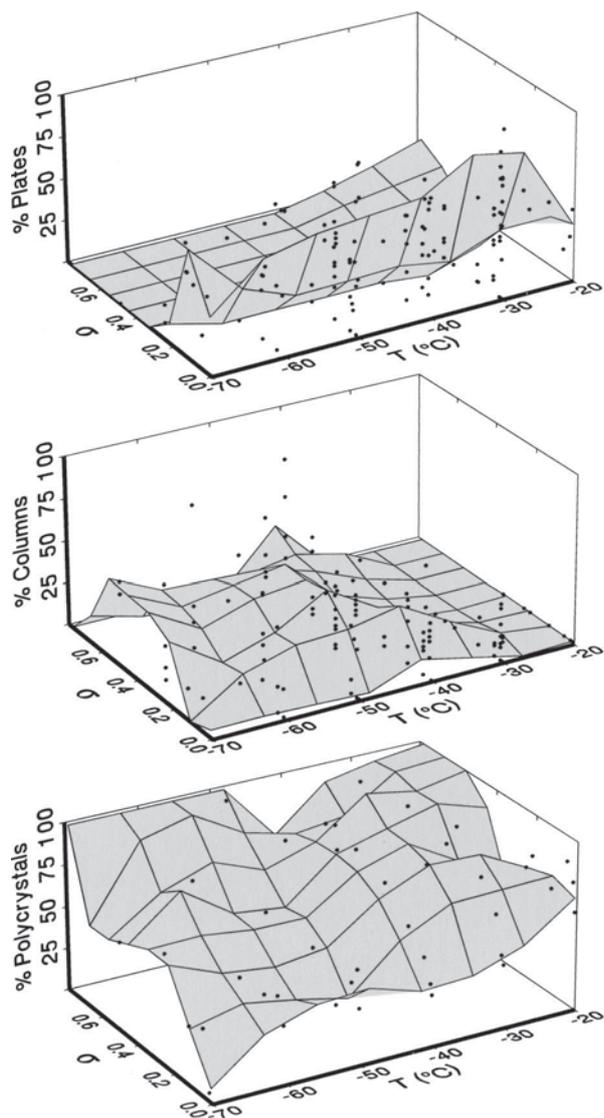
FIG. 16. Surface plot summary of habit distributions for (top) plates, (middle) columns, and (bottom) polycrystals.

1959). However, crystals in this study at times had smooth well-formed facets on all sides while fully incorporating the glass filament obliquely through their volume, as if they were oblivious to the presence of the filament. While the possibility of growth stimulation from substrate contact cannot be investigated with the current experimental method, the good agreement between habits and growth rates observed in this study in comparison with our own fall tower (Barkey et al. 2002) and other substrate-free experiments performed near −20°C (Yamashita et al. 1984; Fukuta and Takahashi 1999; Bacon et al. 2003), in addition to atmospheric in situ observations at lower temperatures, appear to indicate that the substrate has a minor effect on growth characteristics, especially when crystals are grown to

sizes that well exceed that of the substrate as is the case in this study.

5. Comparison with atmospheric in situ observations

The growth rates and habit results presented in section 3 represent crystals growing under conditions of constant temperature and mean ice supersaturation. While such conditions can occur in the atmosphere for limited periods of time, crystals often experience variable growth conditions due to sedimentation, varying updrafts and the inhomogeneous distribution of water vapor. Under these conditions, crystal habit and temperature may be poorly correlated. For instance, Stith et al. (2002) sampled crystals in updraft regions of strongly convective tropical clouds at −43°C that were almost exclusively platelike and included stellar plates that normally grow at a temperature around −18°C. The observation of this stellar habit would appear to indicate a very low ice supersaturation in the updraft if this habit did originate at −18°C, otherwise, the habit should have been substantially modified.

Liou et al. (2002) retrieved optical depths in cirrus clouds with cloud tops at 10–11 km and cloud base as low as 8 km using a parameterization of light scattering by columnar crystals. Cloud systems with this range of altitudes typically contain the habit transition near −40°C in their upper regions resulting in crystal populations of mixed habits with substantially different optical properties. Additionally, columns and bullet rosettes, which fall to the platelike region at temperatures warmer than −40°C, are modified by the change in growth conditions, becoming increasingly hollow with increasing temperature, further altering their optical properties (this modification of habit has recently been simulated in the static diffusion chamber and will be presented elsewhere). The habit transition region near −40°C presents a number of difficulties when comparing laboratory results and atmospheric in situ observations. However, if cloud depth is limited or if conditions do not vary too extensively, reasonably good agreement is obtained as demonstrated in the following case comparisons.

Field et al. (2001) observed crystals in an orographic wave cloud with the Desert Research Institute (DRI) Cloudscope (Meyers and Hallett 2001) after approximately 300 s of growth at a temperature of approximately −30°C following the measurement of water saturation conditions. The particles observed ranged in size from 50 to 125 μm. From the normalized growth rates presented in Fig. 17 at water saturation (an ice supersaturation of 33%), the data indicate a diameter growth rate of 0.33 multiplied by 0.75 μm (sσ)$^{-1}$ for a growth rate of 0.25 μm s^{-1}. After 300 s this would yield an average crystal size of about 75 μm, assuming that at least some of the crystals nucleated by heterogeneous nucleation when water saturation was reached as ob-
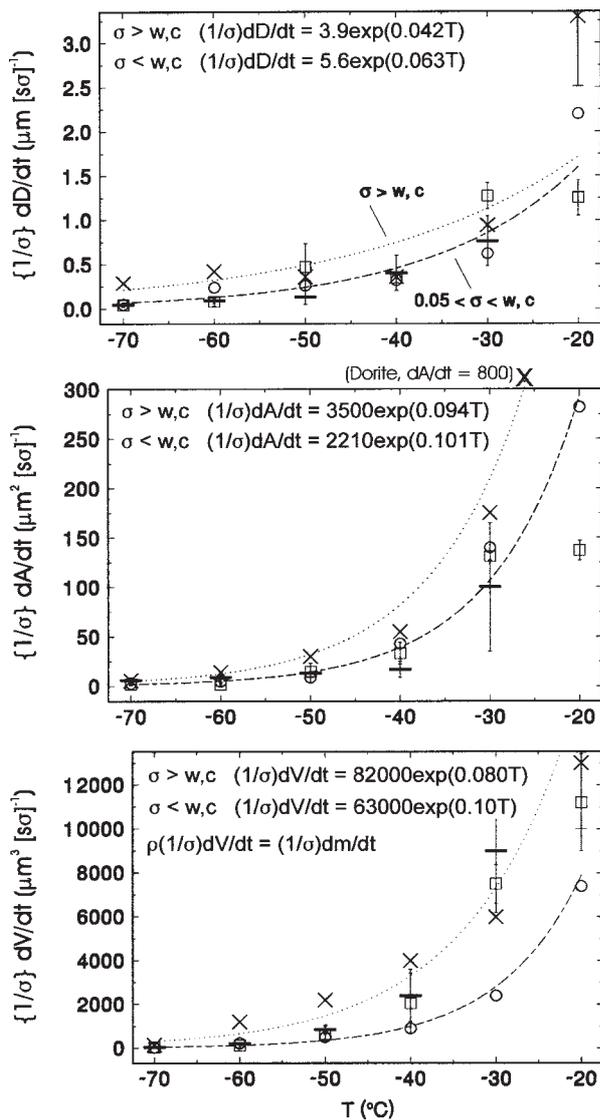
FIG. 17. Exponential fits of average growth rates normalized to ice supersaturation for (top) maximum dimension, (middle) maximum projected area, and (bottom) volume. Lower dashed curve (open circles) represents results for ice supersaturation less than water saturation or the critical supersaturation for nucleation, and the upper dotted curve (crosses) is for higher values. Low ice supersaturation growth results representative of smoothly faceted halo producing crystals are given by open squares (pristine plates) and horizontal bars (pristine columns). Error bars represent the range of growth values rather than the error from the regression analysis.

served in this study. From the variance of the growth results, a spread of sizes of 25–125 μm is expected, an estimation that spans the observed crystal sizes. While the crystals were not clearly resolved (P. R. Field 2002, personal communication), they are assumed to be platelike polycrystals since the temperature was too warm for columns or bullet rosettes.

The results found in aufm Kampe et al. (1951) include

atmospheric in situ observations at temperatures colder than $-25°$C from the pioneering work of Weickmann (1945) performed before World War II in addition to laboratory results obtained from a large cold chamber down to a temperature of $-45°$C. The laboratory cold chamber results confirm the dominant platelike habit observed between $-20°$ and $-40°$C in this work. Weickmann observed ice crystals at the top of a cirrocumulus cloud at $-41°$ and at the bottom of the same cloud at $-37°$C. The habits observed at cloud top were consistent with laboratory results from this study at an ice supersaturation of around 25%–40% (bullet rosettes and columns), the same habits being observed at cloud bottom, though of larger size and exhibiting some modification of habit due to fallout to a warmer platelike regime. At times, bullet rosettes are observed in situ at temperatures warmer than $-40°$C; however, since habit is primarily a function of temperature, the results from this study indicate that such crystals nucleated at colder temperatures above and then were collected at lower warmer regions due to sedimentation.

Observations at the ground also confirm the basic platelike and columnar growth regimes identified in this work. Ohtake and Inoue (1980) observed crystals in the Antarctic, often precipitating from clear skies. In that study it was found that bullet rosettes were typically observed following the incursion of moist air aloft at temperatures between $-40°$ and $-55°$C and often coincided with a high cirrus or cirrostratus cloud layer 2000 to 4500 m above ground level. Complex side plane crystals in addition to bullets and columns were observed when moist upper-air at temperatures between $-30°$ and $-45°$C was present, and thin plates that grew in the lowest 1000 m were observed at temperatures between $-22°$ and $-28°$C. These observations were essentially consistent throughout a year of observations. Similar results observed in Arctic Canada can be found in Kajikawa et al. (1980).

Goodman et al. (1989) observed stratospheric crystals in the Antarctic with the National Aeronautics and Space Administration (NASA) ER-2 research aircraft at temperatures between $-72°$ and $-78°$C at altitudes between approximately 12.5 and 17 km. The crystal observed consisted of both well-formed and partially sublimated columns with maximum sizes of about 80 μm. Since needles or needle rosettes were not observed, this appears to put an upper limit on the supersaturation of about 15%–25%. Based on the results from this study at these ice supersaturations, a growth time of approximately 50–90 min would be required to achieve crystals of this size, a time period not inconsistent with conditions observed from the aircraft. Instrument measurements indicated that the air was subsaturated with respect to ice during all crystal observations; however, extensive thin cirrus was usually present both above and at the altitude of the aircraft. All crystal sampling additionally occurred in regions with a high probability

of mountain wave events, allowing the possibility that crystals were cycled through long periods of growth and sublimation due to wave motion.

6. Conclusions

The experimental results described in this work demonstrate that the complex behavior of ice crystal habit at temperatures colder than $-20°C$ is related not only to temperature and supersaturation but also to the initial nucleation process. The habit is considerably more variable than that at warmer temperatures, especially in the region between $-20°$ and $-40°C$ where some complex polycrystalline forms have shapes that closely resemble many "aggregates" observed in situ. In this region of the atmosphere where mixed phase clouds are typically encountered, nucleation and initial growth occurs at an ice supersaturation close to water saturation, which then diminishes as glaciation rapidly proceeds. From $0°$ to $-40°C$ and near water saturation, the habit changes from plates ($0°$ to $-4°C$) to columns/needles ($-4°$ to $-8°C$) to plate/dendrites ($-12°$ to $-18°C$) to platelike polycrystals/plates ($-18°$ to $-40°C$).

At temperatures colder than $-40°C$, the habit is dominated by polycrystals with columnar characteristics, including bullet rosettes, in addition to plates and columns, the particular habit distribution dependent on ice supersaturation. The ice phase alone is more likely to be present with heterogeneous nucleation capable of initiating crystal growth at supersaturations well below those required for homogeneous nucleation, either for pure water drops or for supercooled solution drops, which are sufficiently diluted. Homogeneous nucleation of dilute solution drops sets an upper limit on the critical supersaturation for nucleation. Growth can continue at low ice supersaturation for extended periods of time depending on the balance between water vapor removal through crystal growth and vapor availability through updraft cooling. This is the real world of cirrus crystals.

For this region of the atmosphere where the measurement of temperature is accurate but that of ice supersaturation is unreliable, laboratory-observed habits, distributions, and growth rates can be used to infer approximate in situ ice supersaturations and growth times, as well as to model the growth histories under specified conditions. The total mass growth rate in a glaciated cloud is determined by an integral over all crystal habits and sizes; however, the more rapidly growing habits may dominate the area/mass and volume growth characteristics in relation to both the ice water content and optical extinction. With the input of knowledge concerning ice nuclei at temperatures warmer than approximately $-40°$ and hygroscopic nuclei at temperatures colder than $-40°C$, spectra of crystal habit, size, area, and mass can in principle be predicted from the laboratory results and a known updraft velocity. Since habits and habit distributions show a supersaturation dependence, the observation of atmospheric in situ habits in comparison with the laboratory results at known supersaturation can likewise yield an estimate of updraft conditions. Conversely, at a known temperature and for an observed crystal habit distribution, size, and concentration, a supersaturation inferred from the observed crystal characteristics may be used to infer vertical velocity.

APPENDIX

Glossary of Crystal Habits

This glossary contains descriptions of the crystal habits observed in this study (**bold**) and described in the figures of this paper with additional references to related habit classifications designated by Magono and Lee (1966), indicated by "M&L." None of the habits are aggregates.

Bullet rosettes. Polycrystal consisting of bullets (columns) radiating from a common growth center; bullets can be solid or hollow (sheaths) and typically are of varying lengths (M&L: C2a).

Crossed plate (cp). Polycrystal consisting of 2 to 4 side planes (half-hexagons, c axis perpendicular to half-plane) radiating from a twin boundary structure (TBS) with specific crossing angles between side planes; $\approx70°$, $110°$, and $180°$.

Dorite. Thin bladelike crystal with rounded tip, gently rippled edges, and no side branching; seen on rare occasions in radiating assemblages of sector plates at temperatures near the limit of the dendritic growth regime ($-17°$ to $-19°C$).

Hexagonal plates (pla). Hexagons with basal face width (w) larger than prism face height (h). Varieties include, most commonly, asymmetric or scalene in shape (unequal prism edge lengths); sectorlike (sector plates); irregular (poorly or partially formed, especially at low ice supersaturation and colder than $-60°C$); basal faces can be smooth surfaced, skeletal (ribbed structures), or irregular due to layer nucleation; plate growth is categorized in this study at times as symmetric thin (**pthn**), symmetric thick (**pthk**), or asymmetric (**pasym**) (M&L: P1a, C1g, C1h, CP3d, G2, G3).

Hexagonal columns (col). Simple hexagons with lengths (L) greater than basal face widths (w); solid or hollow to varying degrees (mostly hollow = sheaths), most often somewhat flattened ("tabular"); short, long, and very long; facets can be

smooth or irregular (M&L: C1e, C1f, G1, N1c, N1d, N1e).

Gohei twin. Bicrystal twin consisting of thin non-hexagonal platelike structures emanating from a TBS forming a chevronlike structure with a tip angle of 77°; simple gohei twins have two platelike components; complex forms appear as repeated, interpenetrating, twin units; they can also appear as component of complex assemblages of crystals.

Irregular (irreg). A generally low ice supersaturation habit consisting of irregularly faceted, thick polyhedra (often incomplete hexagons) in contacting or interpenetrating combinations (M&L: I1, I4).

Irregular assemblage of plates (irreg). Modest to high supersaturation habit (>5%); contacting or interpenetrating combinations of plates with random orientations; components often consist of poorly or partially formed hexagons and/or nonhexagonal platelike shapes (M&L: G6).

Needles. Long, thin, solid, needlelike structures, typically nonhexagonal in shape; tips can be pointed or faceted; can appear in appear in bunches or layered stacks; needles at −60° are more smoothly faceted compared with needles observed at −5°C, which are often irregularly faceted and highly fractured in appearance (M&L: N1a, N1b).

Overlapping parallel plate (opp). *Low supersaturation:* combinations of at least two thick, noncoplanar, overlapping plates (plate centers offset) with parallel crystallographic axes that grow concurrently from a common contact region, slightly interpenetrating in this region. *High supersaturation:* combinations of thin overlapping plates with parallel crystallographic axes radiating from a thin, irregularly shaped, platelike hub, each component slightly interpenetrating with the hub.

Prisms. Ambiguous term describing any refracting crystal (from thin plates to equiaxed to long columns, "thin" and "long" being relative assessments); term rejected by Magono and Lee.

Radiating assemblage of plates. An assemblage of plates radiating from a common polycrystalline growth center (M&L: G5, P7a?).

Rectangular twin. polycrystal twin with two right-triangle-shaped, ribbed, platelike structures growing with each hypotenuse attached to a TBS, which yields the appearance of a rectangle with a pronounced diagonal line; the TBS is typically raised in appearance with small triangular steps emanating from it; one side of each of the large component triangles is typically thick and sometimes develops as a scroll. Not of tetragonal crystal symmetry.

Scroll. Curled, typically six-sided sheathlike structure that does not close on itself as a normal columnar sheath; colder than −20°C, they typically appear along the edges of gohei and rectangular twins in addition to being components of spearhead crystals.

Side plane type (sdpl). Polycrystals with pronounced TBS from which one to several side planes (half-hexagons, *c* axis perpendicular to half-plane) grow; side planes can appear in both symmetric pairs and in asymmetric pairs or singles, staggered in positions along the TBS and sometimes parallel and overlapping with other side planes (M&L: S1; radiating assemblages of side planes: S2, P7a).

Sheath. A column that is hollow for most of its length.

Spearhead (sph). Medium to high ice supersaturation habit; polycrystal repeating twin dominated by growth of the TBS; some have pronounced small to large side plane development while others are "bare" (**shb**); probably related crystallographically to gohei and rectangular twins since they exhibit common features.

Trigonal crystals. Crystals with apparent triangular shape, related to the presence of stacking faults, or hexagons with two trios of equal length sides, one trio of sides being much shorter than the other (facets at the vertices of the "triangle"); typically appear with low frequency (≈5%).

Twin boundary structure (TBS). The microscopic structure apparent in several types of polycrystals and twins (gohei twins, crossed plates, side plane types, spearheads, rectangular twins) that results from defects at the molecular scale that constitute a twinning plane or grain boundary (the interface between two or more contiguous crystals that are not exactly of the same orientation); appearances range from a thin seam to a thick, distorted, quasilinear structure separating crystal components.

REFERENCES

aufm Kampe, H. J., H. K. Weickmann, and J. J. Kelly, 1951: The influence of temperature on the shape of ice crystals growing at water saturation. *J. Meteor.,* **8,** 168–174.

Bacon, N. J., M. B. Baker, and B. D. Swanson, 2003: Initial stages in the morphological evolution of vapour-grown ice crystals: A laboratory investigation. *Quart. J. Roy. Meteor. Soc.,* **129,** 1903–1927.

Bailey, M., and J. Hallett, 2002: Nucleation effects on the habit of vapour grown ice crystals from −18°C to −42°C. *Quart. J. Roy. Meteor. Soc.,* **128,** 1461–1484.

Barkey, B., M. Bailey, K. N. Liou, and J. Hallett, 2002: Light-scattering properties of plate and column ice crystals generated in a laboratory cold chamber. *Appl. Opt.,* **41,** 5792–5796.

Bennett, A., D. Hamilton, A. Maradudin, R. Miller, and J. Murphy, 1965: *Crystals: Perfect and Imperfect.* Walker and Company, 237 pp.

Bryant, G. W., J. Hallett, and B. J. Mason, 1959: The epitaxial growth of ice on single-crystalline substrates. *J. Phys. Chem. Solids,* **12,** 189–195.

Burton, W. K., N. Cabrera, and F. C. Frank, 1951: The growth of crystals and the equilibrium structure of the surfaces. *Philos. Trans. Roy. Soc. London,* **A243,** 299–358.

Chen, J.-P., and D. Lamb, 1994: The theoretical basis for the parameterization of ice crystal habits: Growth by vapor deposition. *J. Atmos. Sci.,* **51,** 1206–1221.

Elliott, W. P., 1971: Dimensions of thermal diffusion chambers. *J. Atmos. Sci.,* **28,** 810–811.

Field, P. R., and Coauthors, 2001: Ice nucleation in orographic wave clouds: Measurements made during INTACC. *Quart. J. Roy. Meteor. Soc.,* **127,** 1493–1512.

Fukuta, N., 1969: Experimental studies on the growth of small ice crystals. *J. Atmos. Sci.,* **26,** 522–531.

——, and T. Takahashi, 1999: The growth of atmospheric ice crystals: A summary of findings in vertical supercooled cloud tunnel studies. *J. Atmos. Sci.,* **56,** 1963–1979.

Furukawa, Y., 1982: Structures and formation mechanisms of snow polycrystals. *J. Meteor. Soc. Japan,* **60,** 535–547.

——, and T. Kobayashi, 1978: On the growth mechanism of polycrystalline snow crystals with a specific grain boundary. *J. Cryst. Growth,* **45,** 57–65.

Gonda, T., 1980: The influence of the diffusion of vapor and heat on the morphology of ice crystals grown from the vapor. *J. Cryst. Growth,* **49,** 173–181.

Goodman, J., O. B. Toon, R. F. Pueschel, K. G. Snetsinger, and S. Verma, 1989: Antarctic stratospheric ice crystals. *J. Geophys. Res.,* **94,** 16 449–16 457.

Hallett, J., 1961: The growth of ice crystals on freshly cleaved covellite surfaces. *Philos. Mag.,* **6,** 1073–1087.

——, 1964: Experimental studies of the crystallization of supercooled water. *J. Atmos. Sci.,* **21,** 671–682.

——, and B. J. Mason, 1958: The influence of temperature and supersaturation on the habit of ice crystals grown from the vapour. *Proc. Roy. Soc. London,* **247A,** 440–453.

——, W. P. Arnott, M. P. Bailey, and J. T. Hallett, 2002: Ice crystals in cirrus. *Cirrus,* D. K. Lynch et al., Eds., Oxford University Press, 480 pp.

Heymsfield, A. J., 1986: Ice particles observed in a cirriform cloud at −83°C and implications for polar stratospheric clouds. *J. Atmos. Sci.,* **43,** 851–855.

——, and R. G. Knollenberg, 1972: Properties of cirrus generating cells. *J. Atmos. Sci.,* **29,** 1358–1366.

——, A. Bansemer, P. L. Field, S. L. Durden, J. L. Stith, J. E. Dye, W. Hall, and C. A. Grainger, 2002a: Observations and parameterizations of particle size distributions in deep tropical cirrus and stratiform precipitating clouds: Results from in situ observations in TRMM field campaigns. *J. Atmos. Sci.,* **59,** 3457–3491.

——, S. Lewis, A. Bansemer, J. Iaquinta, L. M. Miloshevich, M. Kajikawa, C. Twohy, and M. R. Poellot, 2002b: A general approach for deriving the properties of cirrus and stratiform ice cloud particles. *J. Atmos. Sci.,* **59,** 3–29.

Hobbs, P. V., 1974: *Ice Physics.* Oxford University Press, 837 pp.

Kajikawa, M., and A. J. Heymsfield, 1989: Aggregation of ice crystals in cirrus. *J. Atmos. Sci.,* **46,** 3108–3121.

——, K. Kikuchi, and C. Magono, 1980: Frequency of occurrence of peculiar shapes of snow crystals. *J. Meteor. Soc. Japan,* **58,** 416–421.

Keller, V., and J. Hallett, 1982: Influence of air velocity on the habit of ice crystal growth from the vapor. *J. Cryst. Growth,* **49,** 91–106.

Kikuchi, K., 1970: Peculiar shapes of solid precipitation observed at Syowa Station, Antarctica. *J. Meteor. Soc. Japan,* **48,** 243–249.

——, and A. W. Hogan, 1976: Snow crystal observations in summer season at Amundsen-Scott South Pole Station, Antarctica. *J. Fac. Sci. Hokkaido Univ. Ser. 7,* **5,** 1–20.

Kobayashi, T., 1957: Experimental researches on the snow crystal habit and growth by means of a diffusion cloud chamber. *J. Meteor. Soc. Japan,* **35,** 71–80.

——, 1958: On the habit of snow crystals artificially produced at low pressures. *J. Meteor. Soc. Japan,* **36,** 193–208.

——, 1961: The growth of snow crystals at low supersaturation. *Philos. Mag.,* **6,** 1363–1370.

——, Y. Furukawa, K. Kikuchi, and H. Uyeda, 1976: On twinned structures in snow crystals. *J. Cryst. Growth,* **32,** 233–249.

Korolev, A. V., G. A. Isaac, and J. Hallett, 1999: Ice particle habits in Arctic clouds. *Geophys. Res. Lett.,* **26,** 1299–1302.

——, ——, and ——, 2000: Ice particle habits in stratiform clouds. *Quart. J. Roy. Meteor. Soc.,* **126,** 2873–2902.

Kumai, M., 1982: Formation of ice crystals and dissipation of supercooled fog by artificial nucleation, and variation of crystal habit at early growth stages. *J. Appl. Meteor.,* **21,** 579–587.

Liou, K. N., S. C. Ou, Y. Takano, J. Roskovenshy, G. G. Mace, K. Sassen, and M. Poellot, 2002: Remote sensing of three-dimensional inhomogeneous cirrus clouds using satellite and mm-wave cloud radar data. *Geophys. Res. Lett.,* **29,** 1360, doi:10.1029/2002GL014846.

Liu, S. J., H. Huang, and C. H. Woo, 2002: Schwoebel–Ehrlich barrier: From two to three dimensions. *Appl. Phys. Lett.,* **80,** 3295–3297.

Magono, C., and C. W. Lee, 1966: Meteorological classification of natural snow crystals. *J. Fac. Sci. Hokkaido Univ. Ser. 7,* **2,** 321–335.

Mason, B. J., 2002: The role of clouds in the radiative balance of the atmosphere and their effects on climate. *Contemp. Phys.,* **43,** 1–11.

——, G. W. Bryant, and A. P. van den Heuval, 1963: The growth habits and surface structure of ice crystals. *Philos. Mag.,* **8,** 505–526.

Meyers, M., and J. Hallett, 1998: Ice crystal morphology in aircraft contrails and cirrus. *AMS Conf. on Cloud Physics/14th Conf. on Planned and Inadvertent Weather Modification,* Everett, WA, Amer. Meteor. Soc., 17–20.

——, and ——, 2001: Micrometer sized hygroscopic particles in the atmosphere: Aircraft measurement in the Arctic. *J. Geophys. Res.,* **106** (D24), 34 067–34 080.

Nakaya, U., 1954: *Snow Crystals, Natural and Artificial.* Harvard University Press, 510 pp.

Nelson, J., and C. Knight, 1998: Snow crystal habit changes explained by layer nucleation. *J. Atmos. Sci.,* **55,** 1452–1465.

Ohtake, T., and M. Inoue, 1980: Formation mechanism of ice crystal precipitation in the Antarctic atmosphere. *Proc. 8th Int. Conf. on Cloud Physics,* Clermont-Ferrand, France, Amer. Meteor. Soc., 221–224.

Ono, A., 1970: Growth mode of ice crystals in natural clouds. *J. Atmos. Sci.,* **27,** 649–658.

Pruppacher, H. R., and J. D. Klett, 1997: *Microphysics of Clouds and Precipitation.* Kluwer Academic Publisher, 954 pp.

Rottner, D., and G. Vali, 1974: Snow crystal habit at small excesses of vapor density over ice supersaturation. *J. Atmos. Sci.,* **31,** 560–569.

Ryan, B. F., E. R. Wishart, and D. E. Shaw, 1976: The growth rates and densities of ice crystals between −3°C and −21°C. *J. Atmos. Sci.,* **33,** 842–850.

Sato, N., and K. Kikuchi, 1985: Formation mechanisms of snow crystals at low temperature. *Ann. Gaciol.,* **6,** 232–234.

——, and ——, 1989: Crystal structure of typical snow crystals of low temperature types. *J. Meteor. Soc. Japan,* **67,** 521–528.

Schaefer, V. J., 1949: The formation of ice crystals in the laboratory and the atmosphere. *Chem. Rev.,* **44,** 291–320.

Stith, J. L., J. E. Dye, A. Bansemer, A. Heymsfield, C. A. Grainger, W. A. Petersen, and R. Cifelli, 2002: Microphysical observations of tropical clouds. *J. Appl. Meteor.,* **41,** 97–117.

Takahashi, T., E. Tatsuo, G. Wakahama, and N. Fukuta, 1991: Vapor diffusional growth of free-falling snow crystals between −3° and −23°C. *J. Meteor. Soc. Japan,* **69,** 15–30.

Tape, W., 1994: *Atmospheric Halos.* Antarctic Research Series, Vol. 64, Amer. Geophys. Union, 143 pp.

Tomlinson, E. M., and N. Fukuta, 1979: Aspect ratio of thermal diffusion chambers. *J. Atmos. Sci.,* **36,** 1362–1365.

Wang, P. K., 2002: Shape and microdynamics of the ice particles and their effects in cirrus clouds. *Advances in Geophysics,* Vol. 45, Academic Press, 109–152.

Weickmann, H. K., 1945: Formen und bildung atmosphaerischer eiskristalle. *Beitr. Phys. Atmos.,* **28,** 12–52.

Wood, S. E., M. B. Baker, and D. Calhoun, 2001: New model for the vapor growth of hexagonal ice crystals in the atmosphere. *J. Geophys. Res.,* **106,** 4845–4870.

Yamashita, A., A. Asaharu, T. Ohno, and M. Wada, 1984: Ice crystals grown from the vapor at temperatures lower than −15°C. *Proc. Sixth Symp. on Polar Meteorology and Glaciology,* Tokyo, Japan, National Institute of Polar Research, 96–103.